UNIVERSITY OF COLORADO, BOULDER

Wildfire's Impact on Water Quality: Disinfection Byproduct Formation and Heavy Metal Leachability

by

Paul Jeffrey Wilkerson
B.S., University of Nevada, Reno, 2017

A thesis submitted to the
Faculty of the Graduate School of the
University of Colorado in partial fulfillment
of the requirement for the degree of

Master of Science
Department of Civil, Environmental, and Architectural Engineering

2020

This thesis entitled:
Wildfire's Impact on Water Quality: Disinfection Byproduct Formation and Heavy Metal Leachability
written by Paul Jeffrey Wilkerson
has been approved for the Department of Civil, Environmental, and Architectural Engineering

_____
Fernando L. Rosario-Ortiz, Committee Chair

_____
Julia A Korak

_____
Diane McKnight

_____
Date

The final copy of this thesis has been examined by the signatories, and we find that both the content and the form meet acceptable presentation standards of scholarly work in the above-mentioned discipline.

University of Colorado, Boulder

2020

Abstract

Paul Jeffrey Wilkerson

M.S., Department of Civil, Environmental, and Architectural Engineering
Thesis directed by Professor Fernando L. Rosario-Ortiz

Wildfire's Impact on Water Quality: Disinfection Byproduct Formation and Heavy Metal Leachability

Wildfire is a spatially and temporally complex phenomenon that has served a vital role in ecosystem function for millennia. However, drinking water providers have become increasingly aware of wildfire's impacts on the quality of surface water. Increased loads of organic and inorganic constituents, transported by stormflow, are common in streams within burned catchments. As changes in climatic conditions and increased development in wildfire prone areas continues, drinking water providers will need a better understanding of these changes in order to adapt.

Dissolved organic matter (DOM) has the propensity to react with chemical disinfectants to form toxic disinfection byproducts (DBPs). However, wildfire induced chemical changes to DOM can potentially encourage the formation of haloacetonitriles; unregulated DBPs with a lower threshold of toxicity. The goal of the first section in this thesis was to isolate wildfire heating temperature, to better understand how it changes the solubility and reactivity of DOM originating from mineral soil. This was achieved by collecting mineral soil samples from fire prone locations and artificially heating them in a muffle furnace. DOM solubility was heightened at moderate (250°C-350°C) heating temperatures. Additionally, dichloroacetonitrile (DCAN) and dichloroacetic acid (DCAA) formation were stimulated at moderate (250°C) and high (450°C) heating temperatures. To further explore this phenomenon, optical properties were employed to

better understand the intrinsic qualities of DOM. Although we identified some surprising correlations between these optical properties and DBP yield, there is still much work to be done to understand the underlying mechanisms.

Heavy metal contamination can be highly detrimental to the utilitarian and aesthetic qualities of surface water. In several cases, heavy metals have been detected at problematic levels in surface waters as a result of wildfire. However, the concentration and species of these heavy metals is controlled by several complex, spatially heterogenous interactions. Therefore, there exists a need to perform more catchment level studies to contribute knowledge to this complicated issue, as well as inform local water utilities. In the second part of this thesis, the leachability of several heavy metals was assessed from mineral soil and ash samples collected from the Colorado Ryan Fire.

Acknowledgments

I would like to thank everyone that made this thesis possible and supported me through the ups and downs

My advisor Fernando Rosario-Ortiz, for giving me the opportunity to join his outstanding lab group and being an excellent mentor

Diane McKnight and Julie Korak for agreeing to be on my thesis committee, as well as sharing their boundless knowledge

Sarah Fischer and Leah Rivera for all of your help with the Ryan Fire project and the good times we had in the lab

Dorothy Noble for your kindness and willingness to help me work through all of my questions

Rosa (Yun) Yu and Ariel Retuta for sharing so much of their high-quality data. This thesis would have been impossible to finish without their tireless work

Chuck Rhoades, Tim Fegel, and everybody else that have contributed so much of their time to the Ryan Fire project.

Jeff Writer, who's enthusiasm for the outdoors and teaching made every day as a TA exciting

Everybody in the Rosario-Ortiz Lab group, as well as the EVEN program. The only thing better than the research were the friendships I made

Lastly, I would like to thank my parents, my old friends in Reno, and my new friends in Boulder

Contents

Chapter 1 - Background and Research Objectives 1

1.1 Background 1

1.2 Research Objectives 2

Chapter 2 - Impact of Simulated Wildfire on Disinfection Byproduct Formation Potential 4

2.1 Introduction 4

2.2 Methods 7

2.2.1 Soil Sampling 7
2.2.2 Soil Processing 8
2.2.3 Simulated Wildfire Discussion 8
2.2.4 Artificial Heating Methodology 10
2.2.5 Leaching Procedure 10
2.2.6 Dissolved Organic Carbon/Nitrogen 11
2.2.7 WEOC/WEON Analysis 11
2.2.8 Absorbance 12
2.2.9 Chlorination Conditions 12
2.2.10 DBP Analysis 13
2.2.11 Supplemental Optical Measurements Analysis 14
2.2.12 Statistical Analysis 15

2.3 Results 17

2.3.1 DOC and DON 17
2.3.2 Carbonaceous DBP yield 21
2.3.3 Nitrogenous DBP yield 24
2.3.4 $SUVA_{254}$ 25
2.3.5 Adapted Optical Measurements 29

2.4 Discussion 30

2.5 Conclusions 34

Chapter 3 - The Ryan Fire's Impact on the Mobilization of Heavy Metals from Old Growth and Young Forests 36

3.1 Introduction 36

3.2 Methods 39

3.2.1 Site Description and Sample Collection 39
3.2.2 Sample Preparation 39
3.2.3 Leaching Procedure 40
3.2.4 Metals Analysis 41
3.2.5 pH Analysis 41
3.2.7 Statistical Methods 42

3.3 Results and Discussion 43

3.4 Future Work 48

Chapter 4 - Thesis Summary 50

References 52

Appendix I – Chapter 2 Data 62
Appendix II – Chapter 3 Data 73

List of Figures

Figure 2-1. DOC concentration (bars, left y-axis) and WEC (line, right y-axis) in unburned and heated mineral soil samples. Graphs with orange and red bars represent samples from NED and FLG, respectively. Additionally, the subsite can be identified by the letter in the top right corner of each graph. Unburned samples are labeled as control (cntl). Error bars represent the standard deviation of n=4 experimental replicates. Data for these graphs can be found in Table I-1. 17

Figure 2-2. DON concentration (bars, left y-axis) and WEN (line, right y-axis) in unburned and heated mineral soil samples. Graphs with green and blue bars represent samples from NED and FLG, respectively. Additionally, the subsite can be identified by the letter in the top right corner of each graph. Unburned samples are labeled as control (cntl). Error bars represent the standard deviation of n=4 experimental replicates. Data for these graphs can be found in Table I-1. 19

Figure 2-3. The yield of four C-DBPs as heating temperature increased. Samples from NED and FLG are shown as blue and red bars, respectively. The species of DBP is displayed in the upper right corner of each bar graph. The x-axis of each bar graph is identical, however the y-axis range varied between species of DBP. Error bars represent the standard deviation of the three DBP yields for each subsite. Data for these graphs can be found in Table I-2. Additionally, specific DBP yield for each subsite can be viewed in figures I-1 and I-2. 21

Figure 2-4. The yield of two N-DBPs as heating temperature increases. Samples from NED and FLG are shown as blue and red bars, respectively. The species of DBP is displayed in the upper right corner of each bar graph. The x-axis of each bar graph is identical, however the y-axis range varied between species of DBP. Error bars represent the standard deviation of the three DBP yields for each subsite. Data for these graphs can be found in Table I-2. Additionally, specific DBP yield for each subsite can be viewed in figures I-3 and I-4. 24

Figure 2-5. Linear regressions developed between $SUVA_{254}$ and heating temperature. Control $SUVA_{254}$ was removed to improve the linear relationship. This figure with the control $SUVA_{254}$ data can be viewed in figure I-5. P-values for the intercept and coefficient can be found in figure I-4. Lastly, data for these graphs can be found in Table I-2. 25

Figure 2-6. Linear regressions developed between DBP yield and $SUVA_{254}$. P-values for the intercept and coefficient can be found in Table I-5. The linear regression between DCAA yield and $SUVA_{254}$ at NED was improved by removing the outlier (DCAA yield = 199 μg_{DBP} $mg_{DOC}^{-}1$) from the analysis. 27

Figure I-1. C-DBP yield for the three subsites (A, B, and C) at NED. Error bars represent the propagated error calculated from four experimental replicates. 65

Figure I-2. C-DBP yield for the three subsites (D, E, and F) at FLG. Error bars represent the propagated error calculated from four experimental replicates. 66

Figure I-3. N-DBP yield for the three subsites (A, B, and C) at NED. Error bars represent the propagated error calculated from four experimental replicates. 67

Figure I-4. N-DBP yield for the three subsites (D, E, and F) at FLG. Error bars represent the propagated error calculated from four experimental replicates. 67

Figure I-5. Linear regression developed between $SUVA_{254}$ and heating temperature. Unlike figure 2-5, this figure includes $SUVA_{254}$ data for unburned control samples. Note that the linear relationships shown in this figure

are poorer than the ones shown in figure 2-5. P-values for the intercept and coefficient can be viewed in table I-4. 68

Figure II-1. Linearity test used to determine a mass/volume ratio for leaching Ryan Fire mineral soil and ash samples. Mass units are in g, while volume is in mL. 73

Figure II-2. Kinetics test used to determine the optimal leaching time. Twelve hours was chosen due to the maximum DOC concentration occurring at this time interval. The decrease measured between twelve and 48 hours could be due to instrument accuracy or sorption of DOC to the walls of the plastic centrifuge tube. 73

List of Tables

Table 2-1. The four intrinsic optical measurements linearly regressed against DBP yield. SpA, SpC, and apparent fluorescence quantum yield (Φf) were adapted from a study by McKay et al., which analyzed samples from the same locations (McKay et al., 2020). Additionally, SUVA254 was both measured by the authors and adapted from the previously mentioned study. 15

Table 2-2. Linear regressions developed between DBP yield and the optical measurements adapted from McKay et al. In the linear equations, Y represents DBP yield and X represents the optical property. Data used to develop these relationships can be found in Table I-6. 29

Table 3-1. The primary and secondary MCLs established by the EPA for the heavy metals of interest in this study. Metals without a primary or secondary MCL are currently unregulated in terms of drinking water treatment. Aquatic life recommendations are also presented for freshwater ecosystems. 37

Table 3-2. pH, DOC concentration, and heavy metals concentrations measured in the Ryan Fire samples. Standard deviations were calculated from three experimental replicates. Sample concentrations normalized to mass can be found in Table II-1. Additionally, p-values used to determine significance can also be found in Table II-2. 43

Table I-1. Organic carbon and nitrogen concentration and content, WEC and WEN, and absorbance and $SUVA_{254}$ values in mineral soil samples from each subsite. Values displayed for DOC and DON are the average of n=4 experimental replicates. Values shown for %C and %N are the average of n=2 experimental replicates. WEC and WEN are calculated using Equation 1. 62

Table I-2. DBP concentration measured from each subsite. DBPs not shown in this table exhibited concentrations too low for interest. Values displayed for DBP concentrations are the average of n=4 experimental replicates. 63

Table I-3. DBP yields displayed also displayed in Figures 2-3 and 2-4. Subsite DBP yields were calculated by dividing the DBP concentration by the DOC concentration for every n=4 experimental replicate, and subsequently averaging these four values. NED DBP yield was calculated by averaging the DBP yield from Subsites A, B, and C. FLG DBP yield was calculated the same way, except with sites D, E, and F. It is

important to note that dividing DOC or DON values from Table I-1 by DBP concentrations from Table I-2 will yield slightly different values 64

Table I-4. Linear regression p-values associated with figure 2-4 and I-5. “No control” indicates that control $SUVA_{254}$ data was removed from the linear regression. 68

Table I-5. Linear regression p-values associated with Figure 2-5. 69

Table I-6. Optical property data adapted from McKay et al. (2020). 69

Table I-7. Two sample, two-tailed t-test p-values used for determining significant differences between DOC and DON concentrations at various temperatures. 70

Table I-8. Two sample, two-tailed t-test p-values used for determining significant differences between NED DBP yields at different heating temperatures. 72

Table I-9. Two sample, two-tailed t-test p-values used for determining significant differences between FLGDBP yields at different heating temperatures. 72

Table I-10. Two sample, two-tailed t-test p-values used for determining significant differences between FLG DBP yield and NED DBP yield. 72

Table II-1. Summary table of pH, DOC, and heavy metals concertation normalized to soil mass. It is important to note that the mass/volume was ratio was constant for all samples. Error is the standard deviation calculated from three experimental replicates. 74

Table II-2. P-values associated with the two sample, two tailed t-tests performed between the various sample types. 75

Equation(s)

WEC/WEN (1) ……...……..…..... 11

List of Acronyms

Φ_f – Apparent Fluorescence Quantum Yield

C-DBP – Carbonaceous Disinfection Byproduct

DBP – Disinfection Byproduct

DOC – Dissolved Organic Carbon

DOM – Dissolved Organic Matter

DON – Dissolved Organic Nitrogen

FLG – Flagstaff Mountain

FP – Formation Potential

GC-ECD – Gas Chromatography with an Electron Capture Detector

HAA – Haloacetic Acid

HAN – Haloacetonitrile

ICP-MS – Inductively Coupled Plasma – Mass Spectrometry

MCL – Maximum Contaminant Level

MDL – Minimum Detection Limit

N-DBP – Nitrogenous Disinfection Byproduct

NED – Nederland

OG – Old Growth Forest

SEC – Size Exclusion Chromatography

SOM – Soil Organic Matter

SpA – Specific peak intensity in the A region of an EEM diagram

SpC – Specific peak intensity in the C region of an EEM diagram

$SUVA_{254}$ – Specific Ultraviolet Absorbance at 254 nm

TDN – Total Dissolved Nitrogen

THM – Trihalomethane

TIN – Total Inorganic Nitrogen

TON – Total Organic Nitrogen

TTHM – Total Trihalomethane

WEC – Water Extractable Carbon

WEN – Water Extractable Nitrogen

YF – Young Forest

Chapter 1 - Background and Research Objectives

1.1 Background

Wildfires are a natural phenomenon that affects the biogeochemistry of forested catchments in a myriad of ways, while also impacting water resources. Many forested ecosystems have evolved to support unique fire regimes that dictate wildfire's intensity, severity, and return interval (Brown et al. 2015). Additionally, several species of flora have adapted to fire prone landscapes by developing specialized traits, such as the lodgepole pine's fire resistant pine cones (Stevens-Rumann and Morgan 2019). Although the natural services provided by wildfires are essential for carbon and nitrogen cycling (Caldwell et al. 2002; DeLuca et al. 2006; Harden et al. 2002), communities situated within affected zones tend to view wildfire as a nuisance.

In addition to the loss of human life and property, wildfires can degrade water quality, thus threatening the supply of safe drinking water (Hohner et al. 2016; Uzun et al. 2020; Writer et al. 2014). In 2018, the 5- and 10- year average, for acres burned in the United States, was exceeded (National Interagency Fire Center, 2018); spurring concern and skepticism (Doerr and Santín 2016) over the future of wildfire's influence. However, changing climatic conditions and continued urban development in fire prone landscapes (Fried, Torn, and Mills 2004; Jolly et al. 2015) have created an impetus to better understand wildfire's influence on surface waters relied upon for drinking water.

Changes to watershed hydrologic function have been well documented after wildfire. Typically, peak flows in streams are higher and occur more suddenly than streams in unburned catchments (Hallema et al., 2017; Neary et al., 2005). The magnitude of change can often be linked to the severity of the burn event. The term "burn severity" has broadly been used to refer to the ecological changes spurred by wildfire; however, many studies use it as a metric to describe the

amount of organic material consumed above and below ground (Keeley, 2009; Neary et al., 2005). Assigning an adjective, such as “low”, “moderate”, or “high”, to a wildfire’s severity tends to be left to the discretion of the author. Wildfire severity is controlled by factors such as burn temperature, oxygen availability, and burn duration (Beadle, 1940; Keeley, 2009). Additionally, fire regime factors, such as meteorological conditions, fuel type, topography, and anthropogenic disturbances, can further influence severity. Higher severity wildfires can completely remove forest floor litter and canopy vegetation, thus decreasing evapotranspiration and runoff interception rates (White et al., 2006). Specific wildfire conditions can also encourage soil hydrophobicity, which effectively decreases infiltration (Bryant et al., 2005). Accordingly, the runoff generated by these factors transports sediment and ash to proximal waterbodies. Entangled within the ash and sediment is a complex mixture of organic and inorganic compounds that ultimately diminish the quality of surface water resources.

1.2 Research Objectives

This thesis is divided into two chapters; each detailing a unique project focused on wildfire’s impacts on water quality. Each chapter will provide further background on specific water quality issues, as well as discuss methodologies and results. The first chapter is concerned with wildfire’s influence on dissolved organic matter (DOM) solubility and disinfection byproduct (DBP) formation. The objectives of this chapter are to:

1. Employ an artificial burning method to isolate and study the effects heating temperature has on DOM solubility.
2. Quantify the DBP yield of DOM leached from artificially heated mineral soil.
3. Attempt to create linear regressions between thermally altered DOM’s optical properties and heating temperature, as well as DBP yield.

The second chapter is concerned with heavy metal solubility in mineral and ash samples collected from the 2018 Colorado Ryan Fire. This chapter represents a work in progress project, delayed by the 2020 COVID-19 pandemic. Moreover, this project is planned to resume past the date of this manuscript's completion. Regardless, the objectives of this chapter are to:

1. Outline the procedures used to leach wildfire impacted mineral soil and ash samples.
2. Present and discuss current heavy metal, pH, and DOC data.
3. Discuss research goals and analyses planned for the immediate future.

Chapter 2 - Impact of Simulated Wildfire on Disinfection Byproduct Formation Potential

Paul J. Wilkerson, Yun Yu, and Fernando Rosario-Ortiz

2.1 Introduction

Streams in burnt watersheds are often subjected to increased sedimentation (Moody and Martin 2009; Reneau et al. 2007; Writer, Mccleskey, and Murphy 2012), elevated levels of inorganic nitrogen, and higher concentrations of dissolved trace elements (Rhoades, Entwistle, and Butler 2012). However, drinking water providers have become increasingly concerned with wildfire's influence on DOM. DOM is a spatially heterogeneous, complex mixture of autochthonous and allochthonous organic material characterized by thousands of unique chemical structures. Some common compounds that comprise DOM, in ascending order of molecular weight, are amino acids, proteins, carbohydrates, fulvic acids, and humic acids. Accordingly, this wide range of possible compounds makes DOM's structural characteristics largely heterogeneous (Yan et al. 2012). These structures are mostly composed of elemental carbon, oxygen, and hydrogen, however nutrients, such as nitrogen and phosphorus, and other inorganic elements are often amalgamated within DOM (Bolan et al. 2011). Lastly, DOM serves as a large source of dissolved organic carbon (DOC) and nitrogen (DON) for aquatic and forest floor ecosystems.

Despite its ecological importance, DOM creates problems for downstream drinking water providers; the most prominent being its nature to stimulate disinfection byproduct (DBP) formation. DBPs are formed during the disinfection phase of water treatment, in which DBP precursors (i.e DOM) react with the disinfectant (typically chlorine or chloramine) to form halogenated byproducts. Although alternative disinfection schemes are becoming an increasingly

viable option for drinking water treatment, many water utilities are still dependent on chlorine-based disinfectants.

Because of the cyto- and genotoxicity associated with DBPs (Boorman G A 1999), the United States has regulated the concentration allowed in distribution systems since 1979 (Environmental Protection Agency, 2016). However, the most recent set of regulations enacted in 2006 only encapsulates two classes of carbonaceous DBPs (C-DBPs); trihalomethanes (THMs) and haloacetic acids (HAAs) (Environmental Protection Agency, 2016). Some notable species of interest, that have yet to be regulated, are haloacetonitriles (HANs). Since their recognition in the 1980s, interest in HANs has grown due to their heightened cyto- and genotoxicity at lower concentrations, compared to traditional C-DBPs (Daniel et al., 1986; Muellner et al., 2007). Due to the likelihood of there being hundreds, if not thousands, of undiscovered DBPs, the future of DBP research could shift focus from DBP identification to broader surrogate measurements (Richardson and Plewa 2020).

The concentration of DOC and DON are commonly monitored in surface waters used for drinking water. When water utilities are interested in the reactivity of DOC and DON, they often calculate the DBP yield; the ratio of a DBP's concentration divided by the concentration of DOC or DON. Moreover, the species and quantity of DBP formed is reliant on the chemical qualities of DOM (Chang et al., 2013). Due to the vast amount of DOM structures existing simultaneously in surface water, optical properties are often employed as surrogate measurements for predicting DOM's reactivity. $SUVA_{254}$, the absorbance of an aqueous sample at 254 nm divided by the concentration of DOC, is undoubtedly the most commonly employed surrogate measurement. $SUVA_{254}$ has most notably shown promise as a predictive tool for C-DBP formation (Hua et al., 2015; Singer, 1999). However, due to the relative simplicity of $SUVA_{254}$, other optical property

measurements utilizing three-dimensional fluorescence scans are becoming increasingly popular, due to their ability to provide a wider array of information on DOM's chemical character.

Wildfire has the ability to influence both the quantity and quality of DOM, and thus DBP yield. Post-fire DOC concentration tends to vary between streams, with some studies reporting minor changes (Mast and Clow 2008; Mast et al. 2016), and others reporting concentrations significantly higher than unburned reference streams (Mceachern et al. 2000; Smith et al. 2011). A bulk of the post-fire DOC is terrestrially derived and transported to water bodies via precipitation events occurring after the initial burn (Writer, McCleskey, and Murphy 2012). However, oftentimes it is difficult to separate the effects of wildfire from routine hydrologic events (Mast et al. 2016). Similar to DOC, fluxes of DON are also largely variable, with some studies reporting little to no change (Santos et al. 2019) and others observing increased DON concentrations in surface waters from burned catchments (Bladon et al. 2008; Uzun et al. 2020). Lastly, wildfire mineralizes detritus; effectively lowering the elemental carbon and nitrogen content available for transport. However, elevated DOC and DON solubility in mineral soils can potentially offset this loss (Hohner et al. 2019).

Several studies have attempted to quantify post-wildfire DBP yield, however the results are still largely inconsistent. C-DBP yield can either decrease (Jeffrey H. Writer et al., 2014) or increase (Hohner et al., 2016) after a wildfire. Of particular concern is the stimulation of HAN yield; a common observation reported in several recent studies (Hohner et al., 2016; Wang et al., 2015, 2016). Due to the uncertainties, a better understanding of post-wildfire DBP yield is needed. A major challenge is trying to isolate wildfire's traits, such as burn temperature, burn duration, and oxygen availability. Accordingly, many have taken a novel approach to this issue by burning

forest floor litter and mineral soil in a controlled laboratory setting. The methods section of this chapter further discusses options for this approach.

In this study, the authors retrieved mineral soil samples from the A-horizon at two distinct fire prone locations in Colorado's Rocky Mountain Front Range. The samples were artificially burned in a muffle furnace under oxic conditions at a range of temperatures (150°C-550°C) commonly observed in low, moderate, and high severity wildfires. DOM was extracted from the heated soils via a coordinated leaching procedure. DOC, DON, and $SUVA_{254}$ were measured in the leachates to understand DOM solubility and aromaticity. Additionally, the authors chlorinated the leachates and assessed the yield of four THMs, nine HAAs, four HANs, two haloketones, and chloropicrin. Lastly, several other optical measurements were adapted from a previous study analyzing samples from the same locations (McKay et al., 2020). The authors developed linear relationships between these optical properties and specific DBP yield to assess the feasibility of predicting specific DBP yield using optical measurements in a post-wildfire setting.

2.2 Methods

2.2.1 Soil Sampling

Soil samples were collected from two distinct locations within Colorado's Rocky Mountain Front Range; Nederland (NED) and Flagstaff Mountain (FLG). To fully represent the spatial heterogeneity of the immediate areas, triplicate samples were taken 10 m apart. The triplicate measurements were designated as subsites A, B, and C for NED and D, E, and F for FLG. NED is dominated by understory vegetation with no closed canopy. The dominant understory flora within NED is blue grama grass (*Bouteloua gracilis*), needle-and-thread grass (*Hesperostipa comate*), and western wheatgrass (*Pascopyrum smithii*). Flagstaff Mountain contained a prominent coniferous canopy and sparse understory vegetation. The main conifer species in the area are

ponderosa pine, Douglas-fir, and subalpine fir-Engelmann spruce (*Picea engelmannii*, *Abies lasiocarpa*) (Retuta, 2018).

2.2.2 Soil Processing

All soil samples were processed immediately after sampling. Each sample was distributed onto a metal tray at a depth of 1 cm. The samples were then placed into an oven at 100°C for two hours to halt microbial activity and eliminate soil moisture that may compromise the samples during storage. Lastly the samples were passed through a 2 mm (No. 10) stainless steel sieve and a 0.841mm (No. 20) sieve to remove rocks and coarse plant material (Retuta, 2018).

2.2.3 Simulated Wildfire Discussion

Collecting and analyzing ash and soil samples from naturally burned watersheds is a useful way of understanding how wildfires effect landscapes and riverine environments (Burton et al. 2016; Pereira and Úbeda 2010; Stein et al. 2012; White et al. 2006; Writer, Mccleskey, and Murphy 2012)(Hohner et al., 2016; Knicker et al., 2006; Larsen et al., 2009). Ash consists of charred organic material from the O-horizon that can be characterized by designating two visual specifications; black ash (moderate burning) and white ash (severe burning) (Wang et al., 2015). Soil samples are collected from the A-horizon and consist of a mix of mineral and organic constituents.

However, due to the lack of true pre-rainstorm burn sites, the collection of ash and soil from burned watersheds tends to be a challenging task. Wildfires weaken hill slope stability and create water repellant layers within soil, thus creating swells of stormwater erosion directly after burn events. Therefore, there is typically a narrow timespan for sample collection before much of the ash and topsoil is lost to proximal surface waters in the form of dissolved compounds and suspended solids (Smith et al., 2011).

Moreover, solely studying environmental samples lacks the degrees of control necessary for understanding more fundamental concepts. Depending on the goal of a given study, controlling factors like temperature, burn time, and oxygen availability can be highly useful. Prescribed burns and simulated burning techniques in laboratories are popular alternatives because of their ability to control some of these factors. Additionally, thermally treated ash and soil produced from these alternatives can be used to create surrogate water quality samples by leaching natural organic matter into laboratory grade water, until post wildfire stream conditions are matched.

Prescribed burning is useful because of its strong likeness to natural wildfires. However, this option is often limited to lower burn temperatures, due to the challenges associated with controlling high intensity wildfires. For this reason, bench scale approaches are a more popular option because of the higher degree of control over burn temperature, oxygen availability, and duration; but questions arise around these methods' likeness to natural and prescribed burns. For example, Santin et al. found that soil organic matter (SOM) required higher temperatures (600-700 °C) to transform into more aromatic forms during prescribed burning rather than what was previously reported (300-500 °C) from bench scale experiments (Santín et al., 2016).

In order to further understand the observed effects of wildfires on the physicochemical properties of DOC, proper control experiments need to be developed and further research is needed to improve and standardize simulated burn techniques. Nevertheless, a variety of methods have already been put into use in other publications. A conventional bench scale setup involves heating field samples in a muffle furnace (Cawley et al., 2017), however other studies have opted for heating in open pans (Hogue & Inglett, 2012) with heat sources such as heat guns (Wieting et al., 2017). Heat durations are widely variable, with times as low as thirty minutes (Jian et al., 2018) and as high as two hours (Cawley et al., 2017). Different temperature ramp protocols for muffle

furnaces have been developed to asses soil aggregate structure (Jian et al., 2018), or to prevent sudden soil ignition (Fernández et al., 1997). Techniques also exist for homogenizing soils during heating, such as turning samples over every 5 minutes while being treated in a muffle furnace (Bodí et al., 2011). The large variety of methods available to researchers provides ample options, however it also makes comparing results difficult from study to study (Bodí et al., 2014).

2.2.4 Artificial Heating Methodology

In this study, we have chosen to employ a muffle furnace, with samples homogenized and exposed to certain temperatures for 2-hours. Samples were placed in 90 mL porcelain dishes and heated to a range of temperatures using a Lindberg/Blue Box Furnace Model BF51442C with a Lindberg Furnace Power Supply Controller Model 59344. The range of temperatures chosen were 150°C, 250°C, 350°C, 450°C, and 550°C, which are based on typical temperatures experienced by topsoil during wildfire. 550°C was chosen as the high end of the heating range due to the near full mineralization of organic matter. Additionally, the temperature range is chosen to represent three respective severities: low (150°C), moderate (250/350°C), and high (450/550°C) (Retuta, 2018). Samples were held in the oven for two hours under aerobic conditions.

2.2.5 Leaching Procedure

It is important to note that DOM solubility can be highly variable between studies due to different protocols, leaching solutions, and the spatial variation of DOM's physicochemical properties. Optimal leaching times were determined through preliminary kinetics tests at a mass/volume ratio of 5 g soil/100mL ultra-pure Milli-Q water. Kinetics tests were carried out by shaking the slurry on a VWR Standard Analog Shaker table for 1, 2, 4, 6, 8, 10, 24, and 48 hours and filtering through a pre-washed 25- mm, 0.45-micron Whatman Puradisc Polyethersulfone syringe filter. Six hours was chosen as the optimal leaching time due to leachate DOC and TDN

concentrations reaching a steady state at this time interval. The process was scaled up to a mass/volume ratio of 5 g soil/1 L ultra-pure Milli-Q water. Leaching times were designated as 6 hours, and samples were filtered through a pre-washed 47- mm, 0.50- micron EMD Millipore Express PLUS Membrane disc filter on a pre-washed glass vacuum filtration apparatus. A larger mass/volume ratio was chosen to provide a greater amount of leachate, and the discrepancy in filter pore size was accepted due to the desire to keep the filter material consistent. Leachates were stored in pre acid washed 1 L amber glass Wheaton bottles at a temperature of 4 °C (Retuta, 2018).

2.2.6 Dissolved Organic Carbon/Nitrogen

DOC and total dissolved nitrogen (TDN) were measured on a Shimadzu TOC-V CSN Total Organic Carbon Analyzer with a TN unit. Both DOC and TDN were measured in replicates of three. TraceMetal Grade hydrochloric acid added to each sample manually to purge inorganic carbon. Total inorganic nitrogen (TIN) was measured calorimetrically at the Arikaree Environmental Laboratory, using a Lachat QuikChem 8500 Flow Injection Module for nitrate and nitrite and a BioTek Synergy 2 Multi-Detection Microplate Reader for ammonium. Total organic nitrogen (TON) was then calculated by subtracting TIN from TDN. Moreover, the authors assumed that TON was equitable to DON (Retuta, 2018).

2.2.7 WEOC/WEON Analysis

Water extractable carbon (WEC) and water extractable nitrogen (WEN) were used to characterize the solubility of DOC and DON as the total carbon and nitrogen content decreased within the soil after heating. The following equation was used to calculate WEC and WEN:

$$\text{WEC or WEN} = \frac{\text{DOC or DON } (\text{mg L}^{-1}) \times V_{\text{leachate}} \text{ (L)}}{M_{\text{solid}} \text{ (mg)} \times \%\text{C or } \%\text{N}} \quad (1)$$

DOC (or DON) are the dissolved organic carbon and nitrogen concentrations of the leachates, $V_{leachate}$ is the leaching volume, M_{soild} is the mass of the solid leached, and %C (or %N) is the carbon (or nitrogen) content of the soil after heating. Data used for WEC and WEN calculations can be viewed in Table I-1. Carbon and nitrogen fractions in the soil were determined using a Thermo Scientific Flash EA1112 Nitrogen and Carbon Analyzer, which employs the Flash Dynamic Combustion method. These analyses were done in replicates of two (Retuta, 2018).

2.2.8 Absorbance

Specific UV absorbance was measured from 200-800nm using a Cary 100 Agilent UV-vis spectrophotometer. A 1-cm pathlength quartz cuvette was used for unburned control samples, as well as samples burned at 150°C, 250°C, and 350°C. Samples burned at 450°C and 550°C were analyzed with a 5-cm path length quartz cuvette. All specific UV measurements were taken in replicates of two (Retuta, 2018). $SUVA_{254}$ was calculated by dividing UV absorbance at 254 nm by the averaged DOC form each subsite. $SUVA_{254}$ reported for NED was calculated as the average of $SUVA_{254}$ values measured at subsites A, B, and C. Accordingly, these calculations were carried out for FLG, except with subsites D, E, and F.

2.2.9 Chlorination Conditions

There are a handful of chlorination conditions used in the past for the analysis of DBPs. Two of the most notable are the Uniform Formation Method (UFC) (Summers et al. 1996) and the DBP Formation Potential Method, the latter being chosen for this study. The conditions selected for chlorination are as follows; initial disinfectant dose = 20 mg/L Free Cl, pH = 7, reaction time = 72 hours, temperature = 20 °C. Before chlorination, leachates were analyzed for DOC and DON and placed into pre-acid washed 250 mL amber glass bottles. A conservative Free Cl residual was chosen as 5 mg/L in order to ensure Free Cl was not the limiting factor. Additionally, some samples

needed to be diluted to remain above this 5 mg/L Free Cl threshold. Chlorine was dosed using a working solution of sodium hypochlorite and ultra-pure DI water. Sample pH was maintained at 7 with a 1M phosphate buffer consisting of reagent grade monobasic and dibasic sodium phosphate. Upon addition of chlorine solution and phosphate buffer, samples were inverted several times and capped using plastic screw caps with Teflon lined septa. Samples were allowed to react for 72 hours in the dark at 20°C.

2.2.10 DBP Analysis

EPA method 551.1 was utilized to analyze four THMs (chloroform ($CHCl_3$), Bromodichloromethane ($CHCl_2Br$), Bromoform ($CHBr_3$), and dibromochloromethane ($CHClBr_2$)), four HANs (bromochloroacetonitrile (BCAN), dibromoacetonitrile (DBAN), dichloroacetonitrile (DCAN), and trichloroacetonitrile (TCAN)), two HKs (1,1-Dichloro-2 propanone and 1,1,1-Trichloro-2-propanone (TCP)), and chloropicrin (ORD US EPA, 1995). Extraction grade pentane was used as the extraction solvent, and Bromofluorobenzene was used as the internal standard. GC-ECD analysis was performed on an Agilent 7890 GC system with micro electron capture detection (ECD), utilizing an Aligent DB-5 column. N_2 was used as the carrier gas at a flow rate of 3.9 mL/min. The injector and detector temperatures were 175°C and 275°C, respectively. The oven programming was as follows; hold at 27°C for 10 minutes, ramp to 41°C at 3°C/min and hold for 6 minutes, ramp to 81°C at 5°C/min, ramp to 180°C at 25°C/min and hold for 6 minutes.

EPA method 552.2 was utilized to analyze nine HAAs; Bromochloroacetic Acid (BCAA), Bromodichloroacetic Acid (BDCAA), Chlordibromoacetic Acid (CDBAA), Dibromoacetic Acid (DBAA), Dichloroacetic Acid (DCAA), Monobromoacetic Acid (MBAA), Monochloroacetic Acid (MCAA), Tribromoacetic Acid (TBAA), Trichloroacetic Acid (TCAA) (EPA, 1995). HAAs

were also analyzed on an Agilent 7890 GC system with micro electron capture detection (ECD), however an Agilent DB-1 column was used. The carrier gas (N_2) flow rate was held at 0.9 mL/min. The injector and detector temperatures were 200°C and 250°C, respectively. The oven programming was as follows; hold at 37°C for 21 minutes, ramp to 136°C at 5°C/min and hold for 3 minutes, ramp to °C at 20°C/min and hold for 3 minutes.

DBP yield is calculated by dividing the DBP concentration by the DOC concentration, except for the (N-DBPs), in which the DBP concentration is divided by the DON concentration. DBP concentrations were measured at each of the subsites for NED (A, B, and C) and FLG (D, E, and F). However, in this manuscript, DBP yield is reported as site averaged values, in which the DBP yield from the three subsites were averaged. Although the means of the three subsites for NED and FLG were deemed significantly different (via one-way ANOVA), the decision to use site averaged values was chosen because the trends exhibited by specific DBP yield as heating temperature increased were visually similar. Specific DBP yield for each subsite can be viewed in figures I-1, I-2, I-3, and I-4.

2.2.11 Supplemental Optical Measurements Analysis

Extrinsic and intrinsic optical property data was adapted from a study by McKay et al., in which the same batch of soil samples from NED and FLG were analyzed (McKay et al., 2020). Extrinsic optical measurements were calculated using data purely from fluorescence and absorbance spectra, while intrinsic optical measurements were calculated by normalizing absorbance and fluorescence data to DOC concentration. Mckay et al. measured absorbance on a Cary-100 Bio UV-Vis spectrophotometer with either 1, 5, or 10 cm quartz cuvettes. Fluorescence was measured in duplicate on a Fluoromax-4 spectrofluorometer. DOC was measured in experimental replicates of four on a Shimadzu TOC-V CSN Total Organic Carbon Analyzer. For

additional details on these methods, consult the *Analytical Methods* section of the publication by McKay et al. To assess the DOM's ability to act as a DBP precursor, linear regression was performed on the yield of each DBP and each optical measurement. Based on an initial analysis, only four intrinsic optical measurements displayed notable linear trends with any of the DBP species. The intrinsic optical measurements of interest are detailed in Table 2-1.

Table 2-1. The four intrinsic optical measurements linearly regressed against DBP yield. SpA, SpC, and apparent fluorescence quantum yield (Φf) were adapted from a study by McKay et al., which analyzed samples from the same locations (McKay et al., 2020). Additionally, SUVA254 was both measured by the authors and adapted from the previously mentioned study.

Optical Property	Spectra	Definition
$SUVA_{254}$	Absorbance	Absorbance at 254 nm divided by DOC concentration.
SpA	Fluorescence	Peak intensity in the A region of an EEM diagram divided by the DOC concentration (Gabor et al., 2014).
SpC	Fluorescence	Peak intensity in the C region of an EEM diagram divided by the DOC concentration (Gabor et al., 2014).
Apparent Fluorescence Quantum Yield (Φ_f)	Fluorescence	Φ_f describes the likelihood of fluorescence occurring in an excited DOM molecule following absorption of a photon. The calculation was performed using Equation (1) from Mckay et al.

2.2.12 Statistical Analysis

Python version 3.8.2, with Scipy, numpy, and matplotlib modules, as well as Microsoft Excel, were used for statistical analysis. DBP yield and $SUVA_{254}$ were reported as the arithmetic mean of three triplicates. Moreover, DBP yield and $SUVA_{254}$ error bars were reported as standard deviation from the arithmetic mean. WEC and WEN error bars were calculated as propagated

error. Statistical significance was determined using a 2-tailed, 2-sample t-test with n_1+n_2-2 degrees of freedom, assuming unequal variance. A significance level of 0.05 was used as a threshold for declaring significance. Accordingly, p-values used for declaring significance can be found in Tables I-7, I-8, I-9, and I-10. Correlations between optical measurements and other metrics were developed via linear regression. Linear correlations were deemed strong if R^2 was greater than 0.70, which is a similar approach utilized by a previous study (Hua et al., 2015). P-values associated with the coefficient (p_{coef}) and intercept (p_{int}) of the linear equations can be found in Tables I-4 and I-5.

2.3 Results

2.3.1 DOC and DON

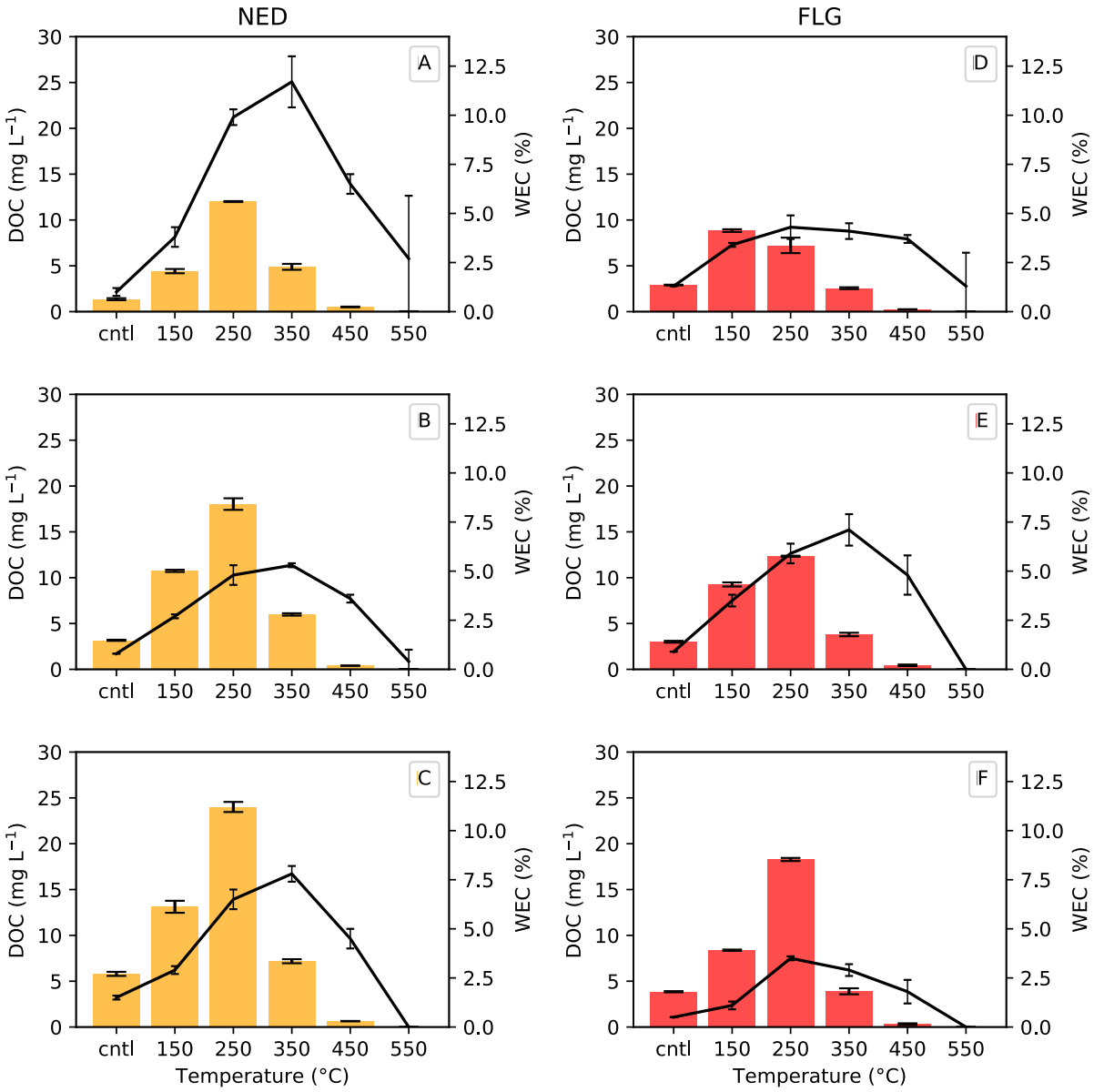

Figure 2-1. DOC concentration (bars, left y-axis) and WEC (line, right y-axis) in unburned and heated mineral soil samples. Graphs with orange and red bars represent samples from NED and FLG, respectively. Additionally, the subsite can be identified by the letter in the top right corner of each graph. Unburned samples are labeled as control (cntl). Error bars represent the standard deviation of n=4 experimental replicates. Data for these graphs can be found in Table I-1.

The range of DOC concentrations observed in the unburned leachates at NED (1.36 mg L^{-1}-5.80 mg L^{-1}) and FLG (2.90 mg L^{-1} to 3.85 mg L^{-1}) were representative of post-snowmelt Colorado streams, based on previously reported ranges (Hood, McKnight, and Williams 2003; Kaushal and Lewis 2005). Heating mineral soil samples from NED and FLG to 150°C and 250°C significantly increased the DOC concentration of the leachates, relative to the control samples. Moreover, heating samples to 350°C from NED significantly increased DOC concentration, while samples from FLG were statistically similar to control samples. Peak DOC concentrations occurred at 250°C for all subsites, except subsite D, in which DOC concentration peaked when heated to 150°C. Mineral soil samples heated to 450°C leached significantly lower concentrations of DOC than control samples. Additionally, the concentration of DOC was far below the minimum detection limit (MDL) in samples heated at 550°C, likely caused by the complete mineralization of organic material (Fernández, Cabaneiro, and Carballas 1997). Peak WEC occurred when samples were heated to 350°C, except subsites D and F, in which the peak was measured at 250°C. Accordingly, peak DOC solubility is achieved when samples were heated to 350°C, despite peak DOC concentrations occurring at 250°C. Lastly, samples from NED frequently leached more DOC, and displayed a higher degree of solubility, than samples from FLG.

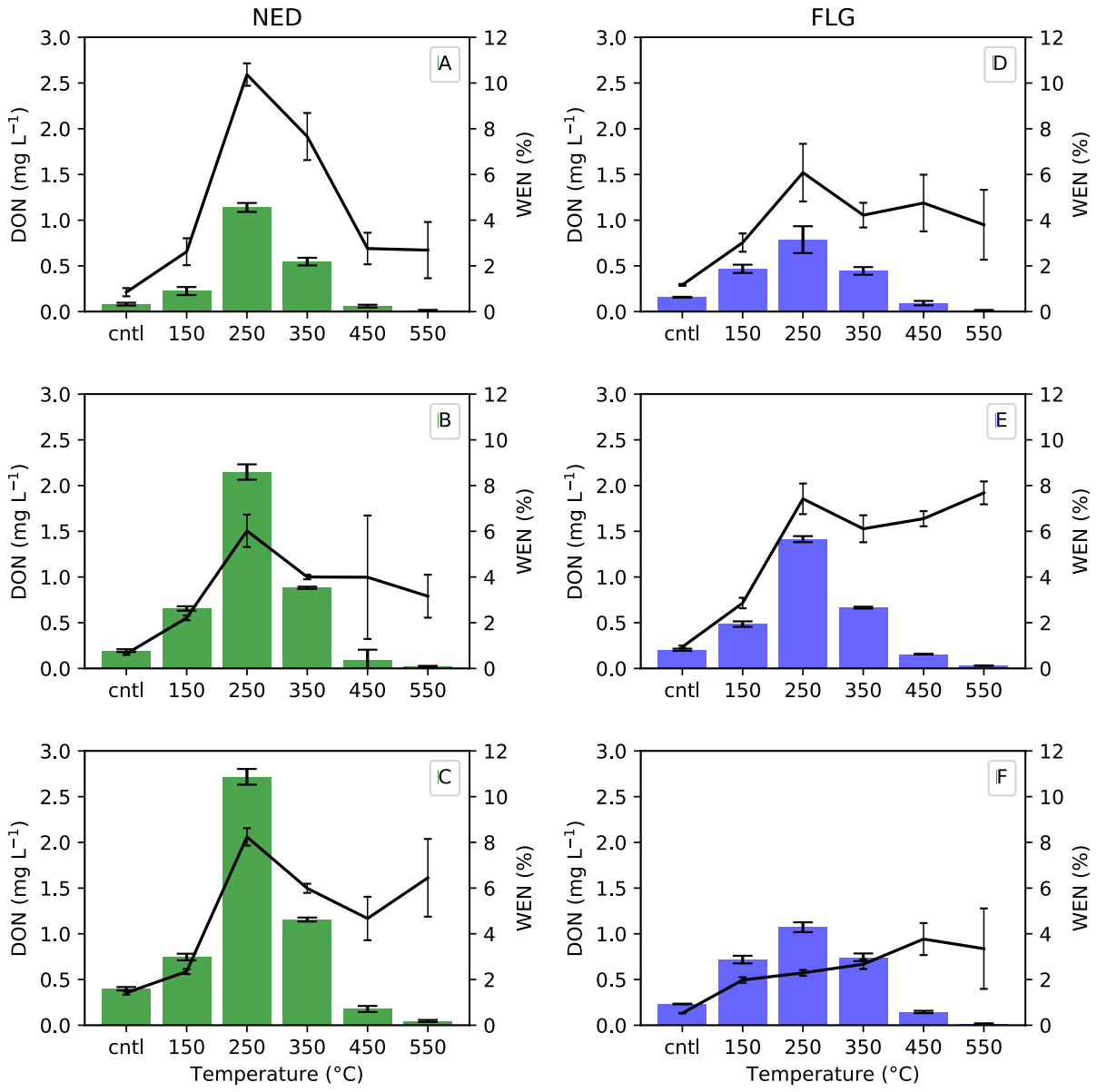

Figure 2-2. DON concentration (bars, left y-axis) and WEN (line, right y-axis) in unburned and heated mineral soil samples. Graphs with green and blue bars represent samples from NED and FLG, respectively. Additionally, the subsite can be identified by the letter in the top right corner of each graph. Unburned samples are labeled as control (cntl). Error bars represent the standard deviation of n=4 experimental replicates. Data for these graphs can be found in Table I-1.

Post-heating DON trends functioned similarly to DOC. DON concentrations from unburned samples ranged from 0.08mg L^{-1}-0.40mg L^{-1} and 0.16mg L^{-1}-0.23 mg L^{-1} for NED and FLG, respectively. Ambient DON concentrations, in Colorado streams with no reported disturbances, have previously ranged from 0.0932 mg L^{-1} to 0.135 mg L^{-1} (Kaushal and Lewis 2005). Samples from NED and FLG had significantly higher DON concentrations, relative to control samples, when heated to 150°C, 250°C, and 350°C. Moreover, peak DON concentrations occurred when samples were heated to 250°C at every subsite. DON concentrations at NED and FLG were significantly lower in samples heated at 450°C, compared to the control, and practically nonexistent in samples heated at 550°C. WEN at NED tended to peak at 250°C, and taper off as heating temperature increased. However, WEN at subsites E and F tended to fluctuate at temperatures above 250°C. Similar to observations made for DOC, samples from NED frequently leached a higher concentration of DON than samples from FLG. Additionally, peak DON solubility tended to be greater at NED, characterized by greater peak WEN values at 250°C.

2.3.2 Carbonaceous DBP yield

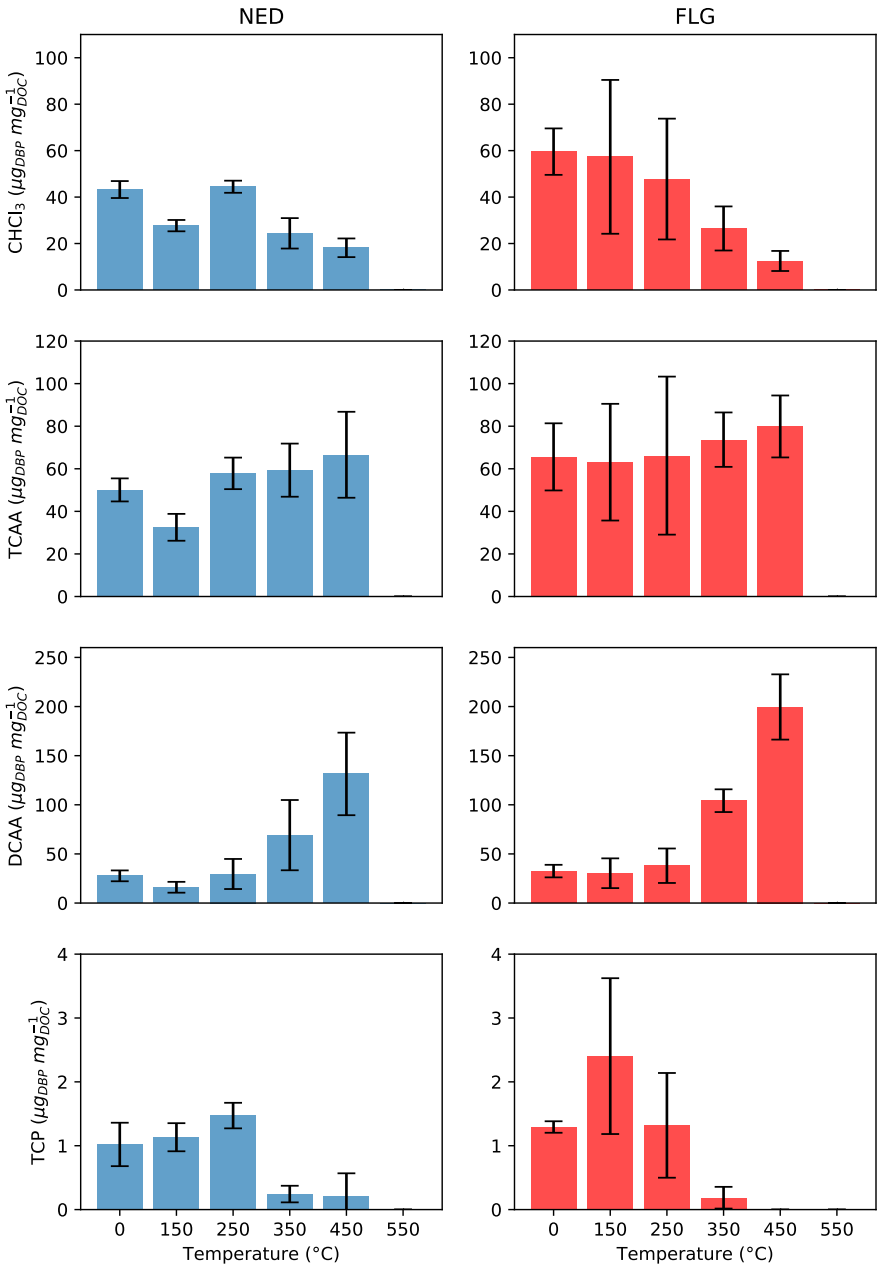

Figure 2-3. The yield of four C-DBPs as heating temperature increased. Samples from NED and FLG are shown as blue and red bars, respectively. The species of DBP is displayed in the upper right corner of each bar graph. The x-axis of each bar graph is identical, however the y-axis range varied between species of DBP. Error bars represent the standard deviation of the three DBP yields for each subsite. Data for these graphs can be found in Table I-2. Additionally, specific DBP yield for each subsite can be viewed in figures I-1 and I-2.

$CHCl_3$ was the dominant THM formed at every heating temperature for both NED and FLG. Trace concentrations of other THMs were formed, however the concentrations were either below the detection limit or below commonly observed values. Therefore, total trihalomethane concentrations (TTHM) are principally constituted of $CHCl_3$. Control $CHCl_3$ yield for both NED and FLG was 43.2 and 59.6 $\mu g_{DBP}\ mg_{DOC}^{-1}$, respectively, which corresponds with a range of $CHCl_3$ yields found in another study utilizing humic isolates and similar chlorination conditions (Reckhow, Singer, and Malcolm 1990). Additionally, control $CHCl_3$ concentrations, measured in samples from NED and FLG, were between the mid and higher range of TTHM concentrations reported by the UFC method after a three day reaction period (Summers et al. 1996). At NED, there was a significant decrease in $CHCl_3$ yield when samples were heated at 150°C, 350°C, and 450°C, relative to the control. However, statistically similar $CHCl_3$ yields were observed between the unheated control samples and samples heated to 250°C. On the other hand, FLG $CHCl_3$ yield did not decrease when heated to 150°C as it did at NED, but rather remained statistically similar to the control. FLG $CHCl_3$ yield did significantly decrease from control to 350°C and 450°C. Both sites did not exhibit any THM formation at 550°C, due to the complete mineralization of DOM. This observation is consistent with all C- and N-DBPs in this study. Lastly, $CHCl_3$ yields tended to be significantly greater at FLG than at NED, however these differences were statistically insignificant. Standard deviations tended to be greater at FLG than NED due to subsite F displaying visibly different trends than subsites D and E, which can be viewed in figure I-2.

HAAs were formed at both sites, the most prominent being TCAA and DCAA. Ranges of control TCAA yield and DCAA yield, at NED and FLG, are consistent with DBP yields reported by another study under similar chlorination conditions (Reckhow et al., 1990). At NED, there was a significant decrease in TCAA yield from control to 150°C, and a significant increase from control

to 350°C and 450°C. As heating temperature increased from the 150°C to 450°C, FLG TCAA yield fluctuated, however none of the fluctuations were deemed significant. Aside from samples heated to 150°C, TCAA yield tended to be statistically similar at both sites for every heating temperature. DCAA yield at NED significantly decreased from control to 150°C and significantly increased when heated to 350°C and 450°C. FLG DCAA yield did not experience the same decrease from control to 150°C, however there was a significant increase from control to 350°C and 450°C. To summarize, TCAA tended to dominate HAA formation at temperatures below 450°C for both sites, while DCAA dominated when soils were heated at 450°C. Moreover, DCAA yield tended to be similar at both sites when samples were heated between 0°C-250°C, and greater at FLG at temperatures between 350-450°C, however this difference was statistically insignificant. Lastly, standard deviations for specific TCAA yield tended to be greater at FLG than NED, due to subsite F displaying visually different trends than subsites D and E, which can be viewed in figure I-2.

TCP was the only haloketone formed at observable concentrations for both sites. The concentrations of TCP measured in this study are generally higher than concentrations measured by Korshin et al., however due to interest in TCP being relatively recent, standard yields have not been well established (Korshin et al., 2007). NED TCP yield significantly increased from control to 250°C, and significantly decreased from control to 350°C and 450°C. Moreover, FLG TCP yield significantly increased from control to 150°C, and significantly decreased from control to 350°C and 450°C. Overall, TCP yields did not significantly differ between sites.

2.3.3 Nitrogenous DBP yield

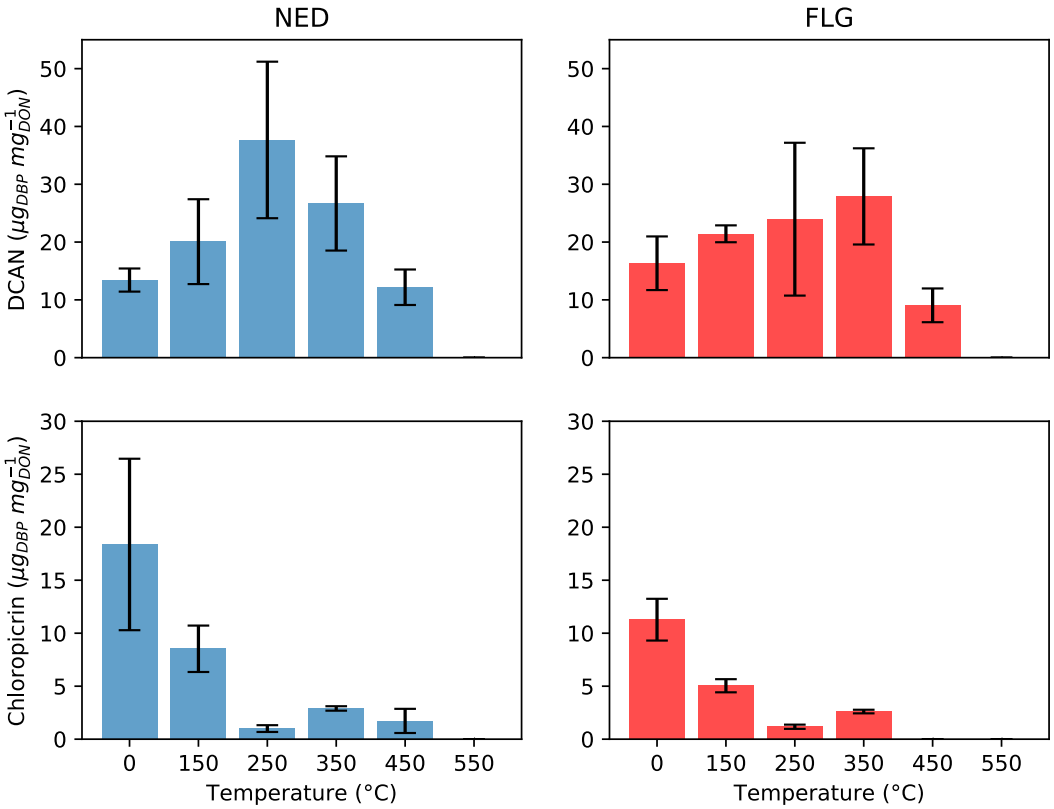

Figure 2-4. The yield of two N-DBPs as heating temperature increases. Samples from NED and FLG are shown as blue and red bars, respectively. The species of DBP is displayed in the upper right corner of each bar graph. The x-axis of each bar graph is identical, however the y-axis range varied between species of DBP. Error bars represent the standard deviation of the three DBP yields for each subsite. Data for these graphs can be found in Table I-2. Additionally, specific DBP yield for each subsite can be viewed in figures I-3 and I-4.

DCAN, TCAN, and chloropicrin were formed at both sites, however TCAN was not elaborated on due to low concentrations and high variability. Control DCAN concentrations were comparatively lower than DCAN concentrations observed under similar conditions (Reckhow et al. 2001). At NED, DCAN yield significantly increased from control to 250°C and 350°C, with peak yield occurring in samples heated to 250°C. FLG DCAN yield also significantly increased from control to 250°C and 350°C, however the peak occurred when samples were heated to 350°C.

However, it should be noted that the relatively large standard deviations at FLG make distinguishing DCAN yield difficult between 150°C and 350°C. Samples heated to 450°C displayed statistically similar and lower DCAN yields for NED and FLG, respectively. Lastly, DCAN yield was similar at both sites, except at 250°C, in which DCAN yield at NED was significantly higher. Chloropicrin yield significantly decreased when samples were heated to any of the temperature, regardless of site. Moreover, chloropicrin yields in unburned samples were higher at NED, compared to FLG, however these differences were statistically insignificant.

2.3.4 $SUVA_{254}$

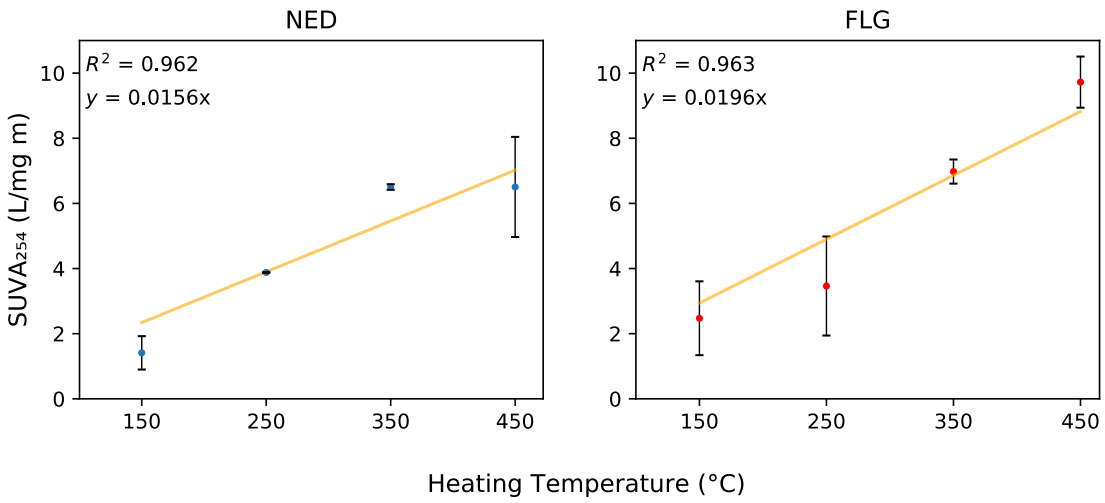

Figure 2-5. Linear regressions developed between $SUVA_{254}$ and heating temperature. Control $SUVA_{254}$ was removed to improve the linear relationship. This figure with the control $SUVA_{254}$ data can be viewed in figure I-5. P-values for the intercept and coefficient can be found in figure I-4. Lastly, data for these graphs can be found in Table I-2.

Samples heated at 550°C were not included in the $SUVA_{254}$ analysis due to the complete combustion of organic matter. $SUVA_{254}$ displayed a positive linear trend as heating temperature increased from 150°C to 450°C, at NED and FLG. A consistent, albeit insignificant, decrease in $SUVA_{254}$ occurred when the samples were heated to 150°C, relative to the unburned samples. This

behavior was also noted by another study observing DOM from the same sites (McKay, Hohner, and Rosario-Ortiz 2020). It is suspected this occurrence is attributed to the soil processing procedure, in which unburned samples were dried at 100°C. For this reason, control $SUVA_{254}$ values were removed from the linear regression shown in figure 2-5. Lastly, $SUVA_{254}$ values were relatively high (> 5.00 L mg_{DOC}^{-1} m^{-1}) in samples heated above 250°C. This could be indication of inorganic interferences (such as iron), however the authors believe these values are indicative of low molecular weight, aromatic compounds formed by heating (Cawley et al., 2017; McKay et al., 2020; Thurman et al., 2020). Regardless, future work should consider measuring the concentration of inorganics to prove this conjecture.

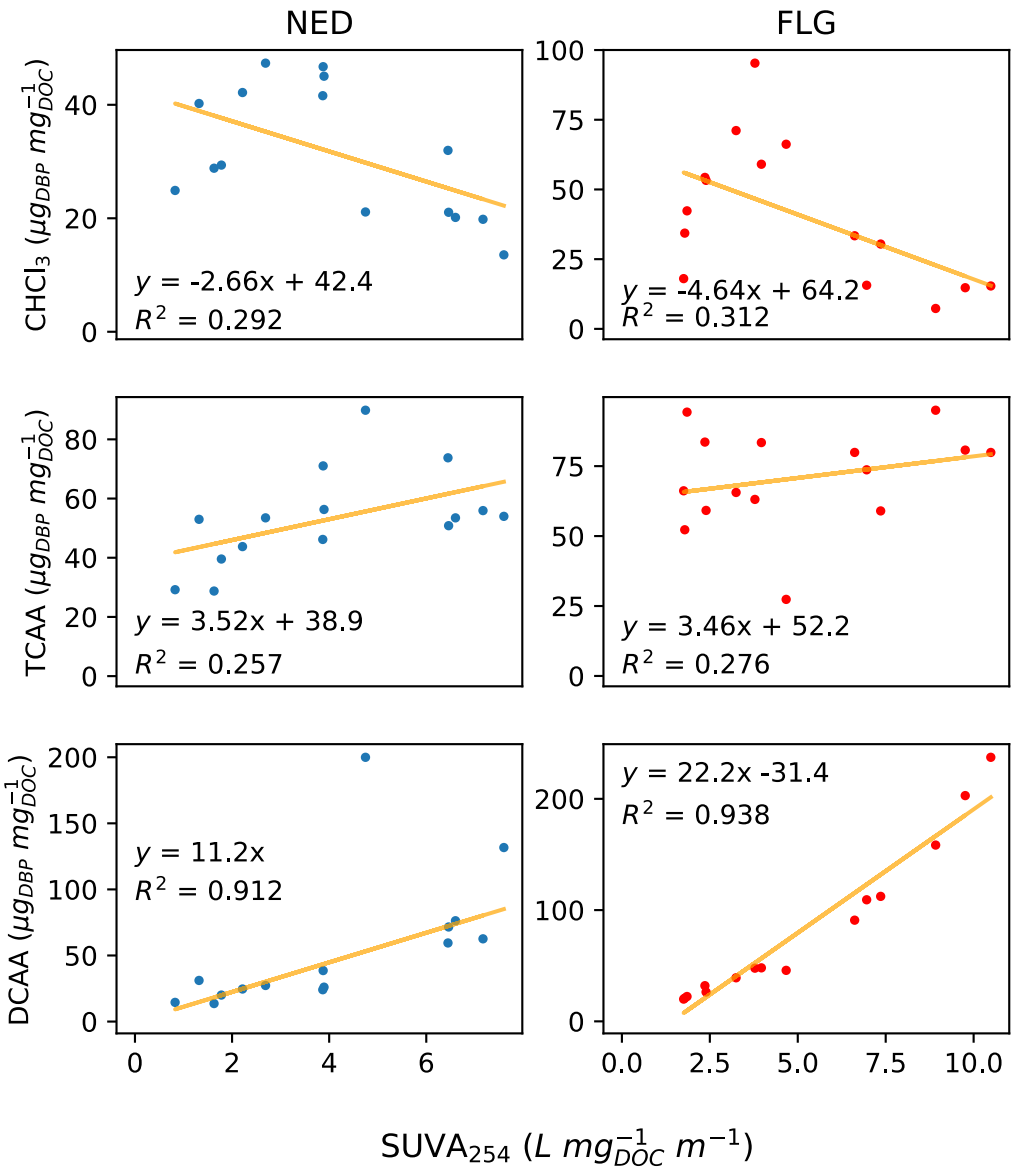

Figure 2-6. Linear regressions developed between DBP yield and $SUVA_{254}$. P-values for the intercept and coefficient can be found in Table I-5. The linear regression between DCAA yield and $SUVA_{254}$ at NED was improved by removing the outlier (DCAA yield = 199 μg_{DBP} mg_{DOC}^{-1}) from the analysis.

For both NED and FLG, $CHCl_3$ yield displayed a negative linear trend with $SUVA_{254}$, while both TCAA yield and DCAA yield displayed positive linear trends. The negative regression between $CHCl_3$ yield and $SUVA_{254}$ contrasts the positive linear relationship observed in previous

studies (Chow et al. 2008; Hua, Reckhow, and Abusallout 2015). On the other hand, the positive linear relationship between the yield of the two HAAs and $SUVA_{254}$ corroborates with observations from the previously mentioned studies (Chow et al. 2008; Hua, Reckhow, and Abusallout 2015). The linear relationship between TCP, DCAN, and chloropicrin were explored, however the trends were either non-existent or heavily influenced by leverage points. From observing the R^2 values, the strength of the linear correlations between $CHCl_3$ yield and $SUVA_{254}$, as well as TCAA and $SUVA_{254}$, are quite weak ($R^2<0.70$). However, DCAA yield consistently displayed relatively strong linear correlations with $SUVA_{254}$ at both sites.

2.3.5 Adapted Optical Measurements

Table 2-2. Linear regressions developed between DBP yield and the optical measurements adapted from McKay et al. In the linear equations, Y represents DBP yield and X represents the optical property. Data used to develop these relationships can be found in Table I-6.

Site	DBP	Optical Property	Equation	p_{int}	p_{coef}	R^2
NED	$CHCl_3$	$SUVA_{254}$	Y = -2.18x +41.6	<0.001	0.0491	0.266
NED	$CHCl_3$	SpA	Y= -1.59x + 37.5	<0.001	0.005	0.456
NED	$CHCl_3$	SpC	Y = -4.09x +37.8	<0.001	0.005	0.457
NED	$CHCl_3$	Φ_f	Y = -208x + 41.9	<0.001	0.002	0.536
NED	TCAA	$SUVA_{254}$	Y = 3.76x + 36.0	<0.001	0.013	0.397
NED	TCAA	SpA	Y = 1.76x + 46.8	<0.001	0.042	0.281
NED	TCAA	SpC	Y = 4.64x + 46.2	<0.001	0.036	0.296
NED	TCAA	Φ_f	Y = 41.7x + 234	<0.001	0.023	0.340
NED	DCAA	SUVA254	Y = 12.8x	-	<0.001	0.841
NED	DCAA	SpA	Y = 8.90x + 22.0	0.0365	<0.001	0.707
NED	DCAA	SpC	Y = 28.3x	-	<0.001	0.828
NED	DCAA	Φ_f	Y = 1084x	-	<0.001	0.852
FLG	$CHCl_3$	$SUVA_{254}$	Y = -4.56x + 66.8	<0.001	0.002	0.536
FLG	$CHCl_3$	SpA	Y = -5.33 + 59.5	<0.001	0.002	0.551
FLG	$CHCl_3$	SpC	Y = -11.8 + 59.4	<0.001	0.001	0.557
FLG	$CHCl_3$	Φ_f	Y = -459 + 61.8	<0.001	0.013	0.388
FLG	TCAA	$SUVA_{254}$	Y = 1.57x + 60.8	<0.001	0.252	0.099
FLG	TCAA	SpA	Y = 1.78 x + 63.5	<0.001	0.257	0.097
FLG	TCAA	SpC	Y = 3.94x + 63.5	<0.001	0.255	0.098
FLG	TCAA	Φ_f	Y = 142x + 63.1	<0.001	0.378	0.06
FLG	DCAA	SUVA254	Y = -14.8x	-	<0.001	0.959
FLG	DCAA	SpA	Y = 20.6x	-	<0.001	0.914
FLG	DCAA	SpC	Y = 45.8x	-	<0.001	0.925
FLG	DCAA	Φ_f	Y = 1600x	-	<0.001	0.738

The four intrinsic measurements ($SUVA_{254}$, SpA, SpC, and Φ_f) adopted from McKay et al. visually displayed notable linear trends with the yield of three DBPs; $CHCl_3$, TCAA, and DCAA. Firstly, the linear regressions between DBP yield and $SUVA_{254}$ measured in our study (Figure 2-6) and by McKay et al. (Table 2-2) exhibited fairly similar slope equations, suggesting that the DOM in our samples is optically similar to DOM in this other study's samples. Secondly, previous studies have been interested in correlating DBP yield with SUVA254, with the hope of developing a predictive tool for water providers. In the past, the strength of these correlations have been determined through the use of R^2 (Hua et al., 2015). Using this method, the optical measurements adapted from McKay et al. exhibited a range of behaviors with $CHCl_3$ yield, TCAA yield and DCAA yield. From observing the R^2 values in Table 2-2, TCAA yield and $CHCl_3$ yield displayed the weakest correlations with $SUVA_{254}$, SpA, SpC, and Φ_f. However, DCAA yield tended to demonstrate stronger linear correlations with SpA and SpC. Φ_f did display a moderately strong linear correlation with DCAA yield at NED, however at FLG this relationship was somewhat weaker. Lastly, regressions were performed with a significance level of 0.05. Accordingly, intercepts were assumed to equal zero if p_{int} exceeded 0.05.

2.4 Discussion

Employing an artificial burn technique proved to be a useful method for generating pyrogenically altered mineral soil samples in a reproducible manner. However, in future studies, other factors such as heating duration and oxygen availability should also be considered. Our method's likeness to naturally occurring wildfire is debatable due to the complexity of natural wildfire's regime. Heating temperature, duration, and oxygen availability can vary spatially and temporally over very small increments, which makes mimicking this phenomenon quite complicated. Nonetheless, the authors believe that the findings from this study are intriguing.

Peak DOC and DON concentrations, as well as peak WEC and WEN values, were observed when samples were exposed to low and moderate heating temperatures (150°C-350°C). These trends are consistent with other studies utilizing artificial burn schemes (Hogue and Inglett 2012; Hohner et al. 2019; Santos et al. 2019; Wang, Dahlgren, and Chow 2015). DOC and DON concentrations exhibited relatively low standard deviations, calculated from the four experimental replicates at both sites, for the full range of heating temperatures. Moreover, the propagated error associated with WEC and WEN also tended to be low for samples heated below 450°C. Samples from NED consistently leached more DOC and DON than samples from FLG, possibly explained by the vegetation found within the two sites. Ecosystems with closed canopies tend to accumulate an abundance of OM on the soil surface, however the flora within grassy ecosystems have root systems that can potentially contribute more OM to the mineral horizon (Mason and Zanner 2005).

Although total carbon and nitrogen content has been reported to decrease in heated soils, low to moderate heating temperatures can induce physiochemical changes to soil that effectively increases DOM solubility, thus offsetting the losses to mineralization (Hohner et al. 2019; Santos, Russell, and Berhe 2016). This is consistent with solubility trends from our study. Santos et al. attributes increased DOM solubility, at moderate heating temperatures, to an abundance of oxygen enriched, aliphatic structures (Santos et al., 2016). Moreover, at 225°C, Cawley et al. observed low molecular weight, O-alkyl enriched compounds present when DOC solubility was at its peak (Cawley et al., 2017). However, a recent study found that heating temperatures between 250°C-450°C resulted in the release of higher concentrations of benzoic polycarboxylic acids (BPCAs) and pyridine dicarboxylic acids PCAs (Thurman et al., 2020). N-enrichment of DOM at moderate temperatures has been observed by Cawley et al., however N-enrichment of pyrogenically altered OM could also dually be a function of both heating temperature and the initial nitrogen content of

the DOM (Cawley et al., 2017; Torres-Rojas et al., 2020) . Lastly, physical alterations to the mineral horizon could also partially explain increased DOC and DON solubility (Jian et al. 2018). Future studies should aim to bridge the effects of heat induced physical and chemical changes to mineral soil.

$SUVA_{254}$ data reported from this study, and by McKay et al., both indicate that DOM aromaticity increases as heating temperature increases. McKay et al. also noted that other intrinsic optical measurements (SpA, SpC, and Φ_f) displayed positive linear relationships with heating temperature. These trends are indicative of the creation of condensed structures; compounds formed by the partial burning of flora and humic material, characterized by an abundance of polycyclic aromatic rings (Schmfidt and Noack 2000). Molecular weight was reported to decrease as a result of moderate and high heating temperatures (Cawley et al. 2017; McKay, Hohner, and Rosario-Ortiz 2020). However, a caveat to these findings is that $SUVA_{254}$ is typically positively correlated with molecular weight (Mostafa et al. 2014; Cawley et al. 2017; McKay, Hohner, and Rosario-Ortiz 2020). Accordingly, more research is needed studying the intrinsic and extrinsic properties of pyrogenically altered DOM.

Depending on the species of DBP analyzed in our study, DBP yield was either unchanged, significantly increased, or significantly decreased by heating temperature. $CHCl_3$ yield gradually decreased as temperature increased at both NED and FLG. Wang et al. also observed this result from chlorinating DOM, derived from naturally burned ashes, generated by varying levels of wildfire intensity (Wang et al., 2015). Moreover, under controlled laboratory heating, overall THM yield has been reported to decrease as heating temperatures ascended from 50°C to 400°C (Wang, Dahlgren, and Chow 2015). THM formation is stimulated by high molecular weight, hydrophobic, terrestrially derived precursors (Marais et al. 2019). Although the optical measurements in this

study indicate aromatic, humic derived DOM, $CHCl_3$ is negatively, albeit weakly, correlated with $SUVA_{254}$, SpA, SpC, and Φ_f. This makes the authors assume that molecular weight could be influencing $CHCl_3$ yield, however further analysis is needed to prove this assumption. However, it should be noted that previous studies have questioned the usefulness of $SUVA_{254}$ as a useful indicator for THM formation (Hua, Reckhow, and Abusallout 2015; Nikolaou et al. 2004; Weishaar et al. 2003). Specifically, Weishaar et al. noted that the reactivity of DOM with NaOCl is highly variable in samples that exhibit similar $SUVA_{254}$ values. This suggests that using $SUVA_{254}$ as a predictive tool for DBP formation might be an overstep of its actual function

Our reported HAA yield trends do not corroborate with studies monitoring streams in naturally burned catchments, or from studies chlorinating leachates created from naturally burned ashes (Hohner et al. 2016; Wang et al. 2015). However, Cawley et al. found total HAA yield was elevated in leachates when soil samples were heated to 225°C in a muffle furnace (Cawley et al., 2017). TCAA yield remained relatively unchanged for all heating temperatures, except when DOM was completely mineralized at 550°C. Moreover, DCAA yield continually increased as heating temperature increased from 150°C to 450°C. Surprisingly, TCAA yield was weakly correlated with $SUVA_{254}$ ($R^2 < 0.7$), which contradicts the strong linear relationship previously recorded (Hua et al., 2015). Additionally, linear correlations between TCAA yield and SpA, SpC, and Φ_f were also relatively weak and displayed visually uninteresting linear regressions. This finding is surprising because TCAA precursors tend to be terrestrially derived hydrophobic precursors (Hua & Reckhow, 2007). On the other hand, DCAA yield displayed strong, positive linear correlations with $SUVA_{254}$, SpA, SpC, and Φ_f (depending on site). This too is contradictory to previous studies, and is surprising due to DCAA precursors typically consisting of nitrogen rich,

aliphatic, low molecular weight compounds (Croué, Violleau, and Labouyrie 2000; Hua and Reckhow 2007).

Enhanced DCAN yield was observed in samples heated to low and moderate heating temperatures. This observation is also present in studies that monitored surface waters in burned catchments, chlorinated naturally burned ashes, and chlorinated leachates derived from artificial burning experiments. (Cawley et al. 2017; Hohner et al. 2016; Majidzadeh, Wang, and Chow 2015; Wang, Dahlgren, and Chow 2015; Wang et al. 2015). HAN formation typically involves amine-based precursors that tend to be aliphatic in nature (Shah and Mitch 2012). The previously mentioned observations by Cawley et al. on DOM's character at moderate temperature notes the existence of N-enriched aliphatic structures, which could explain why DCAN yield is enhanced at these temperatures (Cawley et al., 2017). Moreover, peak DON solubility was observed at moderate heating temperatures, which could also be another factor. Lastly, chloropicrin has been reported to increase as a result of moderate heating temperatures (Cawley et al., 2017), however in our study, chloropicrin yield rapidly decreased as heating temperature increased.

2.5 Conclusions

Mineral soil samples were collected from two distinct fire prone locations, heated in a muffle furnace to simulate wildfire buring, and leached in ultra-pure DI water. The authors observed increased DOC and DON solubility in mineral soil samples exposed to moderate heating temperatures (250°C-350°C). Additionally, $SUVA_{254}$ was observed to linearly increase as heating temperature increased; suggesting that higher temperatures between 350°C-450°C produces highly aromatic DOM. This observation was consistent with another study investigating the optical properties of DOM, from mineral soil originating from the same locations (McKay, Hohner, and Rosario-Ortiz 2020). Chlorine reactivity of the pyrogencically altered DOM was also assessed.

$CHCl_3$ was the only THM formed, however its yield gradually decreased as heating temperature increased. Of the HAAs analyzed, only TCAA and DCAA were formed at considerable concentrations. TCAA yield did not significantly change as heating temperature was increased; however, DCAA yield displayed a sharp increase at 450°C. TCP yield was also stimulated at low to moderate heating temperatures. Of the nitrogenous DBPs analyzed, only DCAN and chloropicrin were formed. DCAN yield peaked when samples were heated to 250°C, however chloropicrin yield quickly decreased as a result of low heating temperatures. Although the likeness of our method to naturally occurring wildfire is questionable, our results characterize potential changes to DOM character and reactivity as a result of wildfire heating temperature. Lastly, the results we obtained from analyzing both the DBP yields and the optical properties displays how much uncertainty currently exists concerning the chemical nature of pyrogenically altered DOM. Before the COVID-19 pandemic, the authors were exploring the DBP yield of hydrophobic and transphilic fractions isolated from burned soils to further explain these questions. Nonetheless, more mechanistic studies are needed in this area of research.

Chapter 3 - The Ryan Fire's Impact on the Mobilization of Heavy Metals from Old Growth and Young Forests

**This chapter represents a work in progress project that was delayed by the COVID-19 pandemic*

3.1 Introduction

Heavy metals are elements that serve an important role in the diets of humans and other living organisms. However, at certain thresholds, heavy metals can compromise the safety of drinking water resources and cause ecological damage. Heavy metals are defined as metallic elements with relatively high densities compared to water (Tchounwou et al., 2012). However, the definition can also encapsulate particularly dangerous metalloids, such as arsenic (As). Humans can ingest heavy metals by drinking contaminated water or consuming aquatic biota. The latter pathway is made possible by the bioaccumulation of heavy metals through trophic levels (Rajeshkumar & Li, 2018). Ingestion of particularly dangerous heavy metals, such as As, cadmium (Cd), chromium (Cr), mercury (Hg), and lead (Pb), can result in acute poisoning, cognitive impairments, and several other long-lasting illnesses (Jaishankar et al., 2014). Other heavy metals, such as Al, Fe, Mn, Cu, and Zn, are also toxic, however they tend to be innocuous at lower concentrations. In addition to health risks, several of these elements can lessen the aesthetic quality and taste of drinking water. As a result, drinking water providers are required to meet primary and secondary maximum contaminant levels (MCLs), which are shown in Table 3-1. Primary MCLs must be met in order to provide safe drinking water, whereas abiding by secondary MCLs is left to the discretion of the water utility. Heavy metals, such as As, Cd, Hg and Pb, are not essential to human health and thus drinking water treatment strives to completely remove these elements. In addition to drinking water standards, recommendations for aquatic life in freshwater ecosystems are also displayed in Table 3-1.

Table 3-1. The primary and secondary MCLs established by the EPA for the heavy metals of interest in this study. Metals without a primary or secondary MCL are currently unregulated in terms of drinking water treatment. Aquatic life recommendations are also presented for freshwater ecosystems.

Element	MCL (mg L^{-1})	Drinking Water Standard	Aquatic Life (Acute) (μg L^{-1})	Aquatic Life (Chronic) (μg L^{-1})	Reference
Al	0.20	Secondary	-	-	(OW US EPA, 2015a, 2015b)
As	0.01	Primary	340	150	(OW US EPA, 2015b, 2015d)
Cd	0.005	Primary	1.80	0.720	(OW US EPA, 2015b, 2015d)
Co	-	-	-	-	-
Cr	0.10	Primary	16	11	(OW US EPA, 2015b, 2015c)
Cu	1.0	Secondary	-	-	(OW US EPA, 2015a, 2015b)
Fe	0.30	Secondary	-	1000	(OW US EPA, 2015a, 2015b)
Mn	0.05	Secondary	-	-	(OW US EPA, 2015a)
Ni	-	-	470	52	(OW US EPA, 2015b)
Pb	0.15	Primary	82	3.2	(OW US EPA, 2015b, 2015d)
Zn	5.0	Secondary	120	120	(OW US EPA, 2015a, 2015b)

The origin of the metals displayed in Table 3-1 can be both lithogenic and anthropogenic. Common lithogenic metals, such as Al, Fe, and Mn are introduced to aquatic and terrestrial ecosystems through weathering of parent material, soil erosion, volcanic eruption, and atmospheric deposition (Abraham et al., 2017). On the other hand, common anthropogenic metals, such as Cd, Cu, and Pb, are introduced through human activities like fossil fuel combustion, industrial wastewater effluent, and several other inputs (Abraham et al., 2017; Wei & Yang, 2010). The mechanisms that control sorption to particles and absorption by plants is complex and controlled by environmental factors such as pH, redox potential, DOM, and the presence of other metals

(Landre et al., 2009). Although these mechanisms are crucial for understanding metal mobilization, this manuscript will primarily focus on the water quality aspect.

As previously covered, wildfire has the ability to impact water quality in numerous ways. Of major concern is the post-fire mobilization of lithogenic and anthropogenic metals. Wildfire combustion physically and chemically alters metal sequestration sinks, thus allowing for remobilization of metals back into the environment. Remobilization is facilitated by subsequent rainstorms that provide transportation to proximal water bodies. However, the combination of fire regime, environmental factors, and the complex interactions associated with each species of metal makes predicting post-wildfire metal concentrations quite complicated. As a result, past studies have reported several similar and contrasting observations.

Heightened concentrations of Mn and Fe are commonly observed in streams and reservoirs after burning, however the magnitude of these observations varies between sites (Burton et al. 2016; White et al. 2006; Writer and Murphy 2012). Other more toxic heavy metals, such as As, Hg, and Pb, are also detected in streams and stormwater as a result of wildfire (Burton et al., 2016; Stein et al., 2012). Yet it can often be difficult to ascertain if the changes are primarily due to burning. Spatial factors such as plant species distribution and topography further complicate the task of pinpointing the origin of remobilized heavy metals (Pereira & Úbeda, 2010). For these reasons, leaching wildfire impacted soil and ash, rather than sampling directly from surface waters, has become a useful option for studying the mechanisms that effect post-wildfire heavy metal solubility. However, this approach is still limited to only making site specific conclusions.

Overall there is still little consensus over wildfire's impact on the remobilization of heavy metals. For this reason, more catchment scale research studying the metal content of ash and mineral soil is needed to better understand this problem. In this experiment, the author sought to

quantify the concentration of twelve leachable heavy metals in mineral soil and ashes affected by the Colorado Ryan Fire. In addition to heavy metals, DOC concentration and pH were also measured to further characterize the water quality of the leachates. This project is currently still in progress; however, this manuscript presents current findings.

3.2 Methods

3.2.1 Site Description and Sample Collection

**Currently waiting for detailed sample collection methods and further site information from field work team.*

The Ryan fire burned over 19,000 acres, in the Fall of 2018, on the Colorado/Wyoming Stateline in both Jackson and Carbon county (Sanchez, 2018). Mineral layer soil and ash samples were sourced from both old growth (OG) and young (YF) forests that were affected by high severity burns. Old growth forests are relatively undisturbed by anthropogenic influences, whereas the young forests are regenerating from logging operations that occurred sometime in the mid-twentieth century. Additionally, unburned mineral and organic layer samples were collected from old growth forests to use as points of comparison. The six sample types are as follows: OG Min, OG Ash, YF Min, YF Ash, Unburned Min, and Unburned Org. Mineral layer soil samples were collected approximately 10 cm below the soil surface (A- and E-horizons), whereas ashes and organic layer soil were easily scraped off the top of the O-horizon. Ten spatial experimental replicates were sampled from the six sample types, however due to time constraints, only three (n=3) were analyzed per sample type.

3.2.2 Sample Preparation

Soil and ash samples were leached for DOC and water-soluble metal content, as follows. First, any moisture content of solids was determined by pre-weighing then placing soil and ash

samples in an Econotherm Laboratory Oven for four hours at 40°C to remove antecedent moisture. After bringing samples to complete dryness, the samples were stored in acid-washed and combusted glass vials until use. A 0.01 M ionic leaching solution was created in a pre-cleaned 1L PYREX glass bottle by dissolving 99%+ (Trace Metal Grade ACS Reagent) calcium chloride dihydrate ($CaCl_2 \cdot 2H_2O$) into ultra-pure Type I DI water. Utilizing a leaching solution, rather than just DI water, was decided upon to broadly mimic the ionic strength of rainwater. Other ionic solution recipes exist, however the one in this method was chosen based on recommendations from a previous study (Gabor et al., 2015). When not in use, the ionic solution was stored at 4°C.

3.2.3 Leaching Procedure

50 mL plastic VWR centrifuge tubes were used as the vessels for leaching to prevent sorption of metals to the vessel walls. Plasticware utilized for leaching was cleaned by soaking materials in a 1% Citranox/99% Type II DI water bath for twenty-four hours. The plasticware was then moved to a 10% Metals Grade Nitric Acid bath for two hours and rinsed three times with ultra-pure Type I DI water. From a preliminary linearity experiment (Figure II-1), a 4g mass:40mL ionic solution ratio was chosen in order to ensure both DOC and metal ion concentrations would be above instrument detection limits. Higher ratios could not be tested because of the limited volume within the centrifuge tubes. a twelve-hour leaching time was chosen based on preliminary kinetics experiments (Figure II-2). Immediately before leaching, exactly 4 g of each sample was weighed in plastic weigh boats and placed in cleaned 50 mL centrifuge tubes containing 40 mL of ionic solution. Over the twelve-hour period, samples were agitated on a VWR Analogue Standard Shaker at a moderate speed. After the 12 hours elapsed, samples were placed in a Thermo Scientific Sorvall Legend X1 centrifuge at a low speed (230 rpm) for 15 minutes.

Sample leachate was then allocated for both DOC/pH and metals analysis. For DOC/pH analysis, 15 mL of sample was passed through a pre-rinsed 0.45 µM glass fiber filter (Whatman GD/X) into 40 mL amber glass vials. For metals analysis, 15 mL of sample was passed through a pre-rinsed 0.45 µM cellulose acetate filter (Whatman GD/X). Leachate aliquots for metal analysis were immediately acidified with Trace Metal Grade Nitric Acid to a pH < 2. All samples were stored at 4°C until further action.

3.2.4 Metals Analysis

Metals were analyzed via inductively coupled plasma – mass spectrometry (ICP-MS), on an Agilent 7900 with an Ultra High Matrix Introduction (UHMI) system, by the Korak lab at the University of Colorado, Boulder. Either helium (He) or hydrogen (H_2) was used as the reactive gas, depending on the analyte of interest. For every ten samples in a suite, a duplicate and matrix spike was analyzed. Additionally, two DI blanks and two 0.01 M $CaCl_2$ leaching solution blanks were analyzed.

3.2.5 pH Analysis

The pH of unacidified, filtered samples was measured with a Thermo Scientific Orion VersaStar Pro Advanced. Immediately before analysis, a three-point calibration curve was created with three analytical buffers with respective pH values of four, seven, and ten. When not in use, the probe was stored in a KCl preservation solution.

3.2.6 DOC Analysis

DOC was measured on a Sievers 5310 C TOC analyzer approximately seventy-two hours after the leachates were created. Samples were manually pre-filtered and automatically acidified by the instrument. Vials containing ultra-pure DI water were analyzed before and after every five samples to check the baseline signal and to clean the autosampler needle. Additionally, three

continuing calibration samples were analyzed to ensure that instrument accuracy was staying within the laboratory's acceptable range. Lastly, three analytical replicates were analyzed to determine the precision associated with creating and storing the leachates.

3.2.7 Statistical Methods

DOC, pH, and metal concentrations are reported as the arithmetic mean of three spatial experimental replicates of each sample type. Accordingly, error represents the standard deviation of the three spatial experimental replicates. The six sample types are OG Ash, Og Min, YF Ash, YF Min, Unburned Org, and Unburned Min. Statistical analysis was performed using Python version 3.8.2, with the Scipy module, as well as Microsoft Excel. Levene's test was used to determine the equitability of each sample type's variance, using a significance level of 0.05. Accordingly, statistical significance was determined at a significance level of 0.05 using a two-tailed, two-sample t-test with n_1+n_2 -2 degrees of freedom, assuming that equal variances. The null hypothesis stated that the difference between means was statistically insignificant, while the alternative hypothesis stated that the difference between means was statistically significant. The p-values used to determine statistical significance are shown in Table II-2.

3.3 Results and Discussion

Table 3-2. pH, DOC concentration, and heavy metals concentrations measured in the Ryan Fire samples. Standard deviations were calculated from three experimental replicates. Sample concentrations normalized to mass can be found in Table II-1. Additionally, p-values used to determine significance can also be found in Table II-2.

			Metal ($\mu g\ L^{-1}$)								
Sample	**pH**	**DOC ($mg\ L^{-1}$)**	**Al**	**Cd**	**Co**	**Cu**	**Fe**	**Mn**	**Ni**	**Pb**	**Zn**
OG Ash	6.55 ± 1.41	29.2 ± 3.63	798 ± 1360*	< MDL	7.28 ± 11.0	6.60 ± 4.44	261 ± 467	9290 ± 1850*	10.5 ± 16.7	< MDL	529 ± 132*
YF Ash	7.82 ± 0.108	8.18 ± 0.701	14.3± 1.21	< MDL	< MDL	< MDL	< MDL	1600 ± 326*	< MDL	< MDL	267 ± 48.1*
Unburned Org.	7.16 ± 0.248	40.5 ± 6.22	81.9 ±52.2	< MDL	< MDL	3.84 ± 1.43	31.0 ± 22.8	1460 ± 1650*	< MDL	< MDL	769 ± 201*
OG Min	5.57 ± 0.598	14.7 ± 3.29	1230 ± 83.0*	< MDL	20.0 ± 11.5	4.23 ± 3.15	1460 ± 1050	3070 ± 2240*	18.0 ± 4.92	< MDL	568 ± 68.7*
YF Min	5.15 ± 1.09	10.9 ± 10.9	370 ± 539*	< MDL	2.87 ± 2.76	2.65 ± 1.78	279 ± 455	794 ± 555*	8.65 ± 3.48	< MDL	771 ± 497*
Unburned Min.	5.05 ± 1.23	14.0 ± 2.43	1720 ± 1520*	6.11 ± 4.57	5.30 ± 2.33	14.7 ± 12.9	154 ± 39.8	2580 ± 2750*	33.8 ± 17.8	2.05 ± 1.36	893 ± 425*

*Samples with at least one experimental replicate that exceeded the instrument calibration curve range

pH ranged between 6.55-7.82 and 5.05-5.57 in the Unburned Org and Unburned Min samples, respectively. Additionally, pH was significantly higher in Unburned Org samples than in the Unburned Min samples. As displayed by the OG Min and YF Min samples in Table 3-2, pH did not significantly vary between forest types in the mineral layer samples. Relative to the Unburned Org samples, pH was not significantly different in OG Ash samples. However, YF Ash samples did exhibit significantly higher pH values, relative to the Unburned Org samples. Past studies have noted that partially charred organic layer material (i.e. ash) can exhibit higher pH values than unburned detritus, partially due to the deposition of $CaCO_3$ (Goforth et al., 2005). Lastly, the difference between YF Ash and OG Ash was deemed insignificant.

Unburned Org samples leached a significantly higher amount of DOC than Unburned Min samples, due to the greater fraction of detritus in the Unburned Org samples. DOC concentration in OG Min and YF Min samples did not significantly change, relative to the Unburned Min samples. However, the OG Ash and YF Ash samples leached a significantly greater amount of DOC than the Unburned Org samples. Lastly, OG Ash samples leached a significantly greater amount of DOC than the YF Ash samples. However, forest type did not significantly influence DOC concentration in mineral layer samples.

In the author's initial experiment, Al, Mn, and Zn exceeded the instrument's calibration curve limit for a majority of the samples analyzed. Additionally, Ca exceeded this limit for every sample analyzed. Upon analysis of the blanks, the author determined that the exorbitant Ca concentrations were a result of the 0.01 M $CaCl_2$ leaching solution. In future work, samples will be diluted and re-analyzed to confirm the concentrations of Al, Mn, and Zn shown in Table 3-2. However, analytes that are within the calibration range will be kept in order to prevent over dilution in future experiments. Internal standards from the experiment did gradually drift in samples

towards the end of the sampling suite, however this phenomenon is likely due to Ca build-up on the instrument's detector. Ca buildup can cause interferences with the internal standards, in which the mass to charge ratio between Ca and the internal standard are equal, thus causing drift in the internal standard recovery (May & Wiedmeyer, 1998). Despite this interference, internal standard recovery was predominantly within the acceptable recovery limit, aside from some of the samples towards the end of the run. Lastly, only elements above their respective minimum detection limits (MDLs) are reported in Table 3-2. Elements that exceeded the calibration curve range are marked with * in Table3-2. This means that if any one experimental replicate was above the calibration curve range, the sample type was marked accordingly. The following sections summarize the findings for each analyte of interest shown in Table 3-2.

Al – More Al appeared to be leached from mineral layer samples, rather than organic layer samples, however this difference was deemed insignificant. In addition, wildfire burning did not significantly change the amount of Al leached from OG or YF samples in either mineral or organic soil horizons. Al leachates created from mineral layer soil samples exceeded the secondary MCL shown in Table 3-1. Previous research has reported both decreased and increased Al concentrations, as a result of burning, in mineral soil and ash, respectively (Groeschl et al., 1993; Pereira et al., 2011). Based on preliminary results, this element should continue to be of interest due to its abundance in mineral layer soil and its prevalence in other studies.

Cd – Only Unburned Min samples leached Cd concentrations above the MDL. Interestingly, the Cd concentrations leached from the Unburned Min samples were also slightly above the primary MCL and the acute and chronic recommendations for aquatic life, shown in Table 3-1. Increased Cd concentrations in burned catchments have been observed in past studies, however Cd

mobilization was not enhanced as a result of burning in this current set of data (Groeschl, Johnson, and Smith 1993).

Co – Co tended to be more abundant in mineral layer samples, compared to organic layer samples, however these differences were insignificant. The highest Co concentrations occurred in the OG Min samples; however, they were not significantly higher than the unburned mineral samples. Moreover, wildfire burning did not significantly change Co concentrations in any of the samples. Forest type was also insignificant in terms of Co leachability.

Cu – Cu was present in both mineral and organic layer samples. OG Ash samples displayed a greater Cu concentration than the Unburned Org samples, however this increase was not significant. Additionally, Unburned Min samples exhibited higher Cu concentrations than OG Min and YF Min samples, however these relationships were also statistically insignificant. Cu solubility has been observed to increase in soils affected by wildfire, however this was not the case in our study (Jovanovic et al. 2011). Lastly, none of the samples exceeded the Cu MCL in Table 3-1.

Fe – Significantly higher Fe concentrations were leached from Unburned Min samples than Unburned Org samples. However, differences in Fe concentrations between mineral and organic layer soil horizons, in wildfire impacted samples, were insignificant. Both OG Min and YF Min samples leached notably higher, albeit statistically insignificant, Fe concentrations than the Unburned Min samples. Additionally, forest type did not significantly change Fe concentrations in any of the wildfire impacted samples. Lastly, OG Min samples exceeded the Fe MCL and recommendations for aquatic life shown in Table 3-1; thus, attention on post-wildfire Fe solubility should still be warranted in future work.

Mn – Comparing Mn concentration data was difficult because most of the experimental replicates exceeded the calibration curve range. For now, this manuscript will use the values reported in table 3-2 for comparison, however future work should attempt to confirm these values. Firstly, every sample's Mn concentration largely exceeded the secondary MCL shown in Table 3-1. The highest Mn concentrations were reported in OG Ash samples, which were also significantly greater than Unburned Org samples. A study that combusted plant material with a muffle furnace also found that Mn content tended to increase as heating temperature increased (Liodakis et al., 2005). In general, Mn is commonly observed in many studies of this nature (Abraham et al., 2017). Lastly, significantly more Mn was leached from organic layer samples originating from wildfire impacted old growth forests, compared to wildfire impacted young forests.

Ni – Ni was most abundant in mineral layer samples from burned and unburned locations. However, the difference between Unburned Min and wildfire impacted samples (OG Min and YF Min) was insignificant. Although elevated Ni concentrations have been reported streams as a result of wildfire, our results did not find a significant difference in Ni leachability as a result of burning (Burton et al., 2016). Additionally, forest type did not have any significant effect on Ni leachability. Lastly, Ni concentrations never exceeded the acute and chronic recommendations for aquatic life, shown in Table 3-1.

Pb – Pb was not detected in any of the samples except for Unburned Min, however the concentration was far below the MCL displayed in Table 3-1. Unburned Min Pb concentrations also did not exceed aquatic life recommendations; however, by a much smaller margin. Although Pb was mostly undetected in our samples, increased Pb concentrations have been reported in post-wildfire runoff (Stein et al., 2012).

Zn – Much like Mn, most of the experimental replicates exceeded the Zn calibration range. However, as previously explained, Zn data as shown in Table 3-2 will be used sparingly and temporarily until further work validates these values. Zn data was not significantly different between any of the samples and did not exceed the secondary drinking water MCL. However, Zn concentrations in all of our samples exceeded the acute and chronic aquatic life recommendations. Although increased Zn concentrations have been observed in wildfire impacted streams, our data suggests that Zn solubility was not influenced by wildfire burning, forest type, or soil horizon (Burton et al., 2016).

3.4 Future Work

Due to the setbacks caused by the COVID-19 pandemic, there are limited conclusions that can currently be made with the current data. However, there are several goals that this project aims to achieve in the immediate future. Firstly, more ICP-MS analyses are needed before Al, Mn, and Zn can be reliably reported. This will be accomplished by diluting samples to target values within the calibration range. Moreover, there are currently only n=3 samples for the six sample types. However, there is an opportunity to increase this number up to n=10. Doing this could potentially improve standard deviations, and ultimately improve the quality of the data.

Secondly, ash samples, sourced from pile burns within the Frasier experimental forest, are also available for analysis. These samples are stratified into three ash types; red ash, black ash, and white ash. Additionally, the pile burns are representative of prescribed burning, which would be an interesting comparison to the naturally burned Ryan Fire samples. The author has already collected DOC, pH, and metals data from n=3 samples, for each of the three ash categories. However, due to time constraints, the author decided to withhold this data until proper analysis can be performed.

Lastly, in collaboration with Sarah Fischer and Leah Rivera, the author has, and currently is, collecting fluorescence and absorbance derived optical property data from the Ryan fire and pile burn ash samples. This data will provide insight into the chemical character of the DOM leached from these samples. Additionally, there could be potential in linking some of the optical properties with metal solubility.

Chapter 4 - Thesis Summary

The previous chapters sought to increase the current understanding of wildfire's influence on several water quality related issues. Specifically, these issues were centered around wildfire's potential to compromise drinking water resources. The complex changes wildfire induces on landscapes presents a breadth of potential research that engineers and scientists should continue to demystify.

Chapter 2 employed an artificial burn technique to explore DOC and DON solubility, as well as DBP yield as it relates to heating temperature. Firstly, DOC and DON solubility was highest at moderate heating temperature (250°C-350°C); a ubiquitous result observed in several past studies. Secondly, the yield of specific DBP species behaved differently depending on heating temperature. Most notably, DCAN yield and DCAA yield were significantly greater at moderate and high temperature, respectively, compared to unburned samples. Thirdly, $SUVA_{254}$ displayed relatively strong positive correlations with heating temperature and DCAA yield. Moreover, two of the intrinsic fluorescence derived optical properties, SpA and SpC, also displayed relatively strong positive correlations with DCAA yield. However, drawing conclusions from these findings is complicated. DCAA is typically preceded by low molecular weight, aliphatic DBP precursors. Yet aromaticity and DCAA yield increased with temperature and were positively correlated. Additionally, SpA and SpC are representative of humic material, which does not exactly conform with the description of DCAA precursors. Accordingly, more research is needed to understand optical properties relationship with DBP yield after thermal alterations. Future work could consider using additional analyses, such as size exclusion chromatography (SEC), to better understand how molecular weight influences DBP yield. As previously stated, before the COVID-19 pandemic, the author was in the process of collecting and analyzing data from hydrophobic and transphilic

fractions that had been isolated from thermally altered DOM. This data would have provided more understanding on DBP yield reaction pathways after wildfire. Further research should continue perusing this avenue because it could provide crucial understanding of why highly toxic N-DBPs are stimulated at moderate heating temperatures.

Chapter 3 mainly investigated the leachability of heavy metals in mineral soil and ash samples collected from old growth and young forests impacted by the Ryan Fire. Although the project is currently in progress, findings were presented from preliminary data. Al, Fe, Mn, and Zn demonstrated particularly high concentrations in both ash and burnt mineral soil samples. Despite this analyte exceeding the instrument calibration curve, Mn displayed significantly higher concentrations in ashes collected from burnt old growth forests. However, future work is needed to validify analytes that exceeded the calibration curve range. pH demonstrated a tendency to be higher in ash samples, compared to mineral soil samples. This finding is common among ash studies and could be used in future work to better understand heavy metal content from ash. Leachable DOC also tended to be higher in ash samples in burnt young and old growth forests, compared to both unburned samples and burned mineral soil samples. Although no relationships were observed between DOC and any of the heavy metals, DOC should continue to be analyzed in future work due to certain metals forming complexes with SOM. Lastly, several goals for future work have been detailed. The main goals include, but are not limited to, collecting and analyzing optical property data on Ryan Fire samples, increase the number of spatial experimental replicates per sample type, and analyze samples from pile burns to compare and contrast the effects of prescribed fires versus natural wildfire.

References

Abraham, J., Dowling, K., & Florentine, S. (2017). Risk of post-fire metal mobilization into surface water resources: A review. *Science of The Total Environment*, *599–600*, 1740–1755. https://doi.org/10.1016/j.scitotenv.2017.05.096

Beadle, N. C. W. (1940). Soil Temperatures During Forest Fires and Their Effect on the Survival of Vegetation. *Journal of Ecology*, *28*(1), 180–192. JSTOR. https://doi.org/10.2307/2256168

Bodí, M. B., Martin, D. A., Balfour, V. N., Santín, C., Doerr, S. H., Pereira, P., Cerdà, A., & Mataix-Solera, J. (2014). Wildland fire ash: Production, composition and eco-hydro-geomorphic effects. *Earth-Science Reviews*, *130*, 103–127. https://doi.org/10.1016/j.earscirev.2013.12.007

Bodí, M. B., Mataix-Solera, J., Doerr, S. H., & Cerdà, A. (2011). The wettability of ash from burned vegetation and its relationship to Mediterranean plant species type, burn severity and total organic carbon content. *Geoderma*, *160*(3–4), 599–607. https://doi.org/10.1016/j.geoderma.2010.11.009

Bryant, R., Doerr, S. H., & Helbig, M. (2005). Effect of oxygen deprivation on soil hydrophobicity during heating. *International Journal of Wildland Fire*, *14*(4), 449–455. https://doi.org/10.1071/WF05035

Burton, C. A., Hoefen, T. M., Plumlee, G. S., Baumberger, K. L., Backlin, A. R., Gallegos, E., & Fisher, R. N. (2016). Trace Elements in Stormflow, Ash, and Burned Soil following the 2009 Station Fire in Southern California. *PLOS ONE*, *11*(5), e0153372. https://doi.org/10.1371/journal.pone.0153372

Cawley, K. M., Hohner, A. K., Podgorski, D. C., Cooper, W. T., Korak, J. A., & Rosario-Ortiz, F. L. (2017). Molecular and Spectroscopic Characterization of Water Extractable Organic Matter from Thermally Altered Soils Reveal Insight into Disinfection Byproduct Precursors. *Environmental Science & Technology*, *51*(2), 771–779. https://doi.org/10.1021/acs.est.6b05126

Chang, H., Chen, C., & Wang, G. (2013). Characteristics of C-, N-DBPs formation from nitrogen-enriched dissolved organic matter in raw water and treated wastewater effluent. *Water Research*, *47*(8), 2729–2741. https://doi.org/10.1016/j.watres.2013.02.033

Daniel, F. B., Schenck, K. M., Mattox, J. K., Lin, E. L. C., Haas, D. L., & Pereira, M. A. (1986). Genotoxic properties of haloacetonitriles: Drinking water by-products of chlorine disinfection. *Fundamental and Applied Toxicology*, *6*(3), 447–453. https://doi.org/10.1016/0272-0590(86)90218-6

EPA. (1995). *EPA Method 552.2: Determination of Haloacetic Acids and Dalapon Analysis in Drinking Water by Ion Exchange Liquid-Solid Extraction and GC with an Electron Capture*. www.caslab.com/EPA-Method-552_2/

Fernández, I., Cabaneiro, A., & Carballas, T. (1997). Organic matter changes immediately after a wildfire in an atlantic forest soil and comparison with laboratory soil heating. *Soil Biology and Biochemistry*, *29*(1), 1–11. https://doi.org/10.1016/S0038-0717(96)00289-1

Gabor, R. S., Baker, A., McKnight, D. M., & Miller, M. P. (2014). Fluorescence Indices and Their Interpretation. In A. Baker, D. M. Reynolds, J. Lead, P. G. Coble, & R. G. M. Spencer (Eds.), *Aquatic Organic Matter Fluorescence* (pp. 303–338). Cambridge University Press. https://doi.org/10.1017/CBO9781139045452.015

Gabor, R. S., Burns, M. A., Lee, R. H., Elg, J. B., Kemper, C. J., Barnard, H. R., & McKnight, D. M. (2015). Influence of Leaching Solution and Catchment Location on the Fluorescence of Water-Soluble Organic Matter. *Environmental Science & Technology*, *49*(7), 4425–4432. https://doi.org/10.1021/es504881t

Goforth, B. R., Graham, R. C., Hubbert, K. R., Zanner, C. W., & Minnich, R. A. (2005). Spatial distribution and properties of ash and thermally altered soils after high-severity forest fire, southern California. *International Journal of Wildland Fire. 14: 343–354*, *14*, 343–354.

Groeschl, D. A., Johnson, J. E., & Smith, D. W. (1993). Wildfire Effects on Forest Floor and Surface Soil in a Table Mountain Pine-Pitch Pine Forest. *International Journal of Wildland Fire*, *3*(3), 149–154. https://doi.org/10.1071/wf9930149

Hallema, D. W., Sun, G., Bladon, K. D., Norman, S. P., Caldwell, P. V., Liu, Y., & McNulty, S. G. (2017). *Regional patterns of postwildfire streamflow response in the Western United States: The importance of scale-specific connectivity*. https://doi.org/10.1002/hyp.11208

Hogue, B. A., & Inglett, P. W. (2012). Nutrient release from combustion residues of two contrasting herbaceous vegetation types. *Science of The Total Environment*, *431*, 9–19. https://doi.org/10.1016/j.scitotenv.2012.04.074

Hohner, A. K., Cawley, K., Oropeza, J., Summers, R. S., & Rosario-Ortiz, F. L. (2016). Drinking water treatment response following a Colorado wildfire. *Water Research*, *105*, 187–198. https://doi.org/10.1016/j.watres.2016.08.034

Hua, G., & Reckhow, D. A. (2007). Characterization of Disinfection Byproduct Precursors Based on Hydrophobicity and Molecular Size. *Environmental Science & Technology*, *41*(9), 3309–3315. https://doi.org/10.1021/es062178c

Hua, G., Reckhow, D. A., & Abusallout, I. (2015). Correlation between SUVA and DBP formation during chlorination and chloramination of NOM fractions from different sources. *Chemosphere*, *130*, 82–89. https://doi.org/10.1016/j.chemosphere.2015.03.039

Jaishankar, M., Tseten, T., Anbalagan, N., Mathew, B. B., & Beeregowda, K. N. (2014). Toxicity, mechanism and health effects of some heavy metals. *Interdisciplinary Toxicology*, *7*(2), 60–72. https://doi.org/10.2478/intox-2014-0009

Jian, M., Berli, M., & Ghezzehei, T. A. (2018). Soil Structural Degradation During Low-Severity Burns. *Geophysical Research Letters*, *45*(11), 5553–5561. https://doi.org/10.1029/2018GL078053

Keeley, J. E. (2009). Fire intensity, fire severity and burn severity: A brief review and suggested usage. *International Journal of Wildland Fire*, *18*(1), 116. https://doi.org/10.1071/WF07049

Knicker, H., Almendros, G., Gonzalez-Vila, F. J., Gonzalez-Perez, J. A., & Polvillo, O. (2006). Characteristic alterations of quantity and quality of soil organic matter caused by forest fires in continental Mediterranean ecosystems: A solid-state 13C NMR study. *European Journal of Soil Science*, *57*(4), 558–569. https://doi.org/10.1111/j.1365-2389.2006.00814.x

Korshin, G. V., Benjamin, M. M., Chang, H.-S., & Gallard, H. (2007). Examination of NOM Chlorination Reactions by Conventional and Stop-Flow Differential Absorbance Spectroscopy. *Environmental Science & Technology*, *41*(8), 2776–2781. https://doi.org/10.1021/es062268h

Landre, A. L., Watmough, S. A., & Dillon, P. J. (2009). The effects of dissolved organic carbon, acidity and seasonality on metal geochemistry within a forested catchment on the

Precambrian Shield, central Ontario, Canada. *Biogeochemistry*, *93*(3), 271–289. https://doi.org/10.1007/s10533-009-9305-0

Larsen, I. J., MacDonald, L. H., Brown, E., Rough, D., Welsh, M. J., Pietraszek, J. H., Libohova, Z., de Dios Benavides-Solorio, J., & Schaffrath, K. (2009). Causes of Post-Fire Runoff and Erosion: Water Repellency, Cover, or Soil Sealing? *Soil Science Society of America Journal*, *73*(4), 1393–1407. https://doi.org/10.2136/sssaj2007.0432

Liodakis, S., Katsigiannis, G., & Kakali, G. (2005). Ash properties of some dominant Greek forest species. *Thermochimica Acta*, *437*(1), 158–167. https://doi.org/10.1016/j.tca.2005.06.041

May, T. W., & Wiedmeyer, R. H. (1998). A table of polyatomic interferences in ICP-MS. *Atomic Spectroscopy*, *19*(5), 150–155. USGS Publications Warehouse.

McKay, G., Hohner, A. K., & Rosario-Ortiz, F. L. (2020). Use of optical properties for evaluating the presence of pyrogenic organic matter in thermally altered soil leachates. *Environmental Science: Processes & Impacts*. https://doi.org/10.1039/C9EM00413K

Muellner, M. G., Wagner, E. D., McCalla, K., Richardson, S. D., Woo, Y.-T., & Plewa, M. J. (2007). Haloacetonitriles vs. Regulated Haloacetic Acids: Are Nitrogen-Containing DBPs More Toxic? *Environmental Science & Technology*, *41*(2), 645–651. https://doi.org/10.1021/es0617441

Neary, D. G., Ryan, K. C., & DeBano, L. F. (2005). *Wildland fire in ecosystems: Effects of fire on soils and water* (RMRS-GTR-42-V4; p. RMRS-GTR-42-V4). U.S. Department of Agriculture, Forest Service, Rocky Mountain Research Station. https://doi.org/10.2737/RMRS-GTR-42-V4

Pereira, P., & Úbeda, X. (2010). Spatial distribution of heavy metals released from ashes after a wildfire. *Journal of Environmental Engineering and Landscape Management*, *18*(1), 13–22. https://doi.org/10.3846/jeelm.2010.02

Pereira, P., Úbeda, X., Martin, D., Mataix-Solera, J., & Guerrero, C. (2011). Effects of a low severity prescribed fire on water-soluble elements in ash from a cork oak (Quercus suber) forest located in the northeast of the Iberian Peninsula. *Environmental Research*, *111*(2), 237–247. https://doi.org/10.1016/j.envres.2010.09.002

Rajeshkumar, S., & Li, X. (2018). Bioaccumulation of heavy metals in fish species from the Meiliang Bay, Taihu Lake, China. *Toxicology Reports*, *5*, 288–295. https://doi.org/10.1016/j.toxrep.2018.01.007

Reckhow, D. A., Singer, P. C., & Malcolm, R. L. (1990). Chlorination of humic materials: Byproduct formation and chemical interpretations. *Environmental Science & Technology*, *24*(11), 1655–1664. https://doi.org/10.1021/es00081a005

Retuta, A. M. (2018). *Effect of Heating Temperature on Dissolvable Constituents from Soil and Litter Material in the Colorado Front Range*. https://scholar.colorado.edu/concern/graduate_thesis_or_dissertations/pr76f3709

Sanchez, H. (n.d.). *Ryan Fire On Colorado-Wyoming State Line Grows Exponentially Over Weekend*. Colorado Public Radio. Retrieved July 21, 2020, from https://www.cpr.org/2018/09/24/ryan-fire-on-colorado-wyoming-state-line-grows-exponentially-over-weekend/

Santín, C., Doerr, S. H., Merino, A., Bryant, R., & Loader, N. J. (2016). Forest floor chemical transformations in a boreal forest fire and their correlations with temperature and heating duration. *Geoderma*, *264*, 71–80. https://doi.org/10.1016/j.geoderma.2015.09.021

Santos, F., Russell, D., & Berhe, A. A. (2016). Thermal alteration of water extractable organic matter in climosequence soils from the Sierra Nevada, California: Thermally Altered WEOC. *Journal of Geophysical Research: Biogeosciences*, *121*(11), 2877–2885. https://doi.org/10.1002/2016JG003597

Singer, P. C. (1999). Humic Substances as Precursors for Potentially Harmful Disinfection By-Products. *Water Science and Technology; London*, *40*(9), 25–30.

Smith, H. G., Sheridan, G. J., Lane, P. N. J., Nyman, P., & Haydon, S. (2011). Wildfire effects on water quality in forest catchments: A review with implications for water supply. *Journal of Hydrology*, *396*(1–2), 170–192. https://doi.org/10.1016/j.jhydrol.2010.10.043

Stankov Jovanovic, V. P., Ilic, M. D., Markovic, M. S., Mitic, V. D., Nikolic Mandic, S. D., & Stojanovic, G. S. (2011). Wild fire impact on copper, zinc, lead and cadmium distribution in soil and relation with abundance in selected plants of Lamiaceae family from Vidlic Mountain (Serbia). *Chemosphere*, *84*(11), 1584–1591. https://doi.org/10.1016/j.chemosphere.2011.05.048

Stein, E. D., Brown, J. S., Hogue, T. S., Burke, M. P., & Kinoshita, A. (2012). Stormwater contaminant loading following southern California wildfires. *Environmental Toxicology and Chemistry*, *31*(11), 2625–2638. https://doi.org/10.1002/etc.1994

Tchounwou, P. B., Yedjou, C. G., Patlolla, A. K., & Sutton, D. J. (2012). Heavy Metals Toxicity and the Environment. *EXS*, *101*, 133–164. https://doi.org/10.1007/978-3-7643-8340-4_6

Thurman, E. M., Yu, Y., Ferrer, I., Thorn, K. A., & Rosario-Ortiz, F. L. (2020). Molecular Identification of Water-Extractable Organic Carbon from Thermally Heated Soils: C-13 NMR and Accurate Mass Analyses Find Benzene and Pyridine Carboxylic Acids.

Environmental Science & Technology, *54*(5), 2994–3001. https://doi.org/10.1021/acs.est.9b05230

Torres-Rojas, D., Hestrin, R., Solomon, D., Gillespie, A. W., Dynes, J. J., Regier, T. Z., & Lehmann, J. (2020). Nitrogen speciation and transformations in fire-derived organic matter. *Geochimica et Cosmochimica Acta*, *276*, 170–185. https://doi.org/10.1016/j.gca.2020.02.034

US EPA, ORD. (1995). *EPA Method 551.1: Determination of Chlorination Disinfection Byproducts, Chlorinated Solvents, and Halogenated Pesticides/Herbicides in Drinking Water by Liquid-Liquid Extraction and Gas Chromatography With Electron-Capture Detection* [Data and Tools]. /homeland-security-research/epa-method-5511-determination-chlorination-disinfection-byproducts

US EPA, OW. (2015a, September 2). *Secondary Drinking Water Standards: Guidance for Nuisance Chemicals* [Overviews and Factsheets]. US EPA. https://www.epa.gov/sdwa/secondary-drinking-water-standards-guidance-nuisance-chemicals

US EPA, OW. (2015b, September 3). *National Recommended Water Quality Criteria—Aquatic Life Criteria Table* [Data and Tools]. US EPA. https://www.epa.gov/wqc/national-recommended-water-quality-criteria-aquatic-life-criteria-table

US EPA, OW. (2015c, September 22). *Chromium in Drinking Water* [Overviews and Factsheets]. US EPA. https://www.epa.gov/sdwa/chromium-drinking-water

US EPA, OW. (2015d, November 30). *National Primary Drinking Water Regulations* [Overviews and Factsheets]. US EPA. https://www.epa.gov/ground-water-and-drinking-water/national-primary-drinking-water-regulations

Wang, J.-J., Dahlgren, R. A., Erşan, M. S., Karanfil, T., & Chow, A. T. (2015). Wildfire Altering Terrestrial Precursors of Disinfection Byproducts in Forest Detritus. *Environmental Science & Technology*, *49*(10), 5921–5929. https://doi.org/10.1021/es505836m

Wang, J.-J., Dahlgren, R. A., Erşan, M. S., Karanfil, T., & Chow, A. T. (2016). Temporal variations of disinfection byproduct precursors in wildfire detritus. *Water Research*, *99*, 66–73. https://doi.org/10.1016/j.watres.2016.04.030

Wei, B., & Yang, L. (2010). A review of heavy metal contaminations in urban soils, urban road dusts and agricultural soils from China. *Microchemical Journal*, *94*(2), 99–107. https://doi.org/10.1016/j.microc.2009.09.014

White, I., Wade, A., Worthy, M., Mueller, N., Daniell, T., & Wasson, R. (2006). The vulnerability of water supply catchments to bushfires: Impacts of the January 2003 wildfires on the Australian Capital Territory. *Australasian Journal of Water Resources*, *10*(2), 179–194. https://doi.org/10.1080/13241583.2006.11465291

Wieting, C., Ebel, B. A., & Singha, K. (2017). Quantifying the effects of wildfire on changes in soil properties by surface burning of soils from the Boulder Creek Critical Zone Observatory. *Journal of Hydrology: Regional Studies*, *13*, 43–57. https://doi.org/10.1016/j.ejrh.2017.07.006

Writer, Jeffrey H., Hohner, A., Oropeza, J., Schmidt, A., Cawley, K. M., & Rosario-Ortiz, F. L. (2014). Water treatment implications after the High Park Wildfire, Colorado. *Journal - American Water Works Association*, *106*(4), E189–E199. https://doi.org/10.5942/jawwa.2014.106.0055

Writer, J.H., & Murphy, S.F. (2012). *Wildfire effects on source-water quality—Lessons from Fourmile Canyon fire, Colorado, and implications for drinking-water treatment* (U.S. Geological Survey Fact Sheet). USGS. https://pubs.er.usgs.gov/publication/fs20123095

Young, D. R., & Jan, T.-K. (1977). Fire fallout of metals off California. *Marine Pollution Bulletin*, *8*(5), 109–112. https://doi.org/10.1016/0025-326X(77)90133-3

Appendix I – Chapter 2 Data

Table I-1. Organic carbon and nitrogen concentration and content, WEC and WEN, and absorbance and $SUVA_{254}$ values in mineral soil samples from each subsite. Values displayed for DOC and DON are the average of n=4 experimental replicates. Values shown for %C and %N are the average of n=2 experimental replicates. WEC and WEN are calculated using Equation 1.

Site	Subsite	Temp (°C)	DOC (mg/L)	%C	WEC (%)	DON (mg/L)	%N	WEN (%)	UV (1/cm)	SUVA (L/mg m)
NED	A	0	1.36	2.73	0.010	0.08	0.194	0.0085	0.036	2.69
NED	A	150	4.42	2.31	0.038	0.22	0.171	0.0262	0.079	1.78
NED	A	250	12.01	2.43	0.099	1.14	0.220	0.1037	0.466	3.88
NED	A	350	4.89	0.84	0.117	0.55	0.143	0.0766	0.316	6.45
NED	A	450	0.51	0.157	0.065	0.06	0.044	0.0276	0.036	7.17
NED	A	550	0.02	0.015	0.027	0.01	0.009	0.0269	0.003	-
NED	B	0	3.17	8.21	0.008	0.20	0.610	0.0064	0.042	1.32
NED	B	150	10.74	8.01	0.027	0.66	0.595	0.0221	0.089	0.83
NED	B	250	18.03	7.57	0.048	2.15	0.713	0.0602	0.698	3.87
NED	B	350	5.99	2.24	0.053	0.88	0.441	0.0400	0.387	6.46
NED	B	450	0.40	0.220	0.036	0.09	0.055	0.0399	0.019	4.75
NED	B	550	0.01	0.041	0.004	0.02	0.014	0.0316	0.002	-
NED	C	0	5.80	7.59	0.015	0.40	0.562	0.0142	0.129	2.22
NED	C	150	13.12	8.92	0.029	0.75	0.636	0.0235	0.214	1.63
NED	C	250	24.01	7.44	0.065	2.72	0.659	0.0824	0.935	3.89
NED	C	350	7.18	1.85	0.078	1.16	0.386	0.0599	0.474	6.60
NED	C	450	0.64	0.286	0.045	0.18	0.076	0.0467	0.048	7.60
NED	C	550	0.00	0.058	0.000	0.05	0.015	0.0645	0.002	-
FLG	D	0	2.90	4.32	0.013	0.16	0.270	0.0117	0.069	2.39
FLG	D	150	8.84	5.21	0.034	0.47	0.310	0.0302	0.158	1.79
FLG	D	250	7.23	3.33	0.043	0.79	0.259	0.0608	0.287	3.97
FLG	D	350	2.56	1.24	0.041	0.44	0.211	0.0422	0.170	6.62
FLG	D	450	0.25	0.135	0.037	0.09	0.039	0.0475	0.022	8.92
FLG	D	550	0.01	0.022	0.013	0.01	0.007	0.0380	0.007	-
FLG	E	0	3.01	6.93	0.009	0.20	0.437	0.0094	0.071	2.36
FLG	E	150	9.26	5.36	0.035	0.48	0.339	0.0286	0.171	1.85
FLG	E	250	12.34	4.20	0.059	1.41	0.381	0.0742	0.576	4.67
FLG	E	350	3.80	1.07	0.071	0.67	0.218	0.0611	0.279	7.36
FLG	E	450	0.44	0.184	0.048	0.16	0.048	0.0655	0.043	9.76
FLG	E	550	0.00	0.043	0.000	0.03	0.008	0.0768	0.004	-
FLG	F	0	3.85	16.80	0.005	0.23	0.880	0.0053	0.125	3.25
FLG	F	150	8.38	15.28	0.011	0.72	0.724	0.0198	0.317	3.78
FLG	F	250	18.28	10.36	0.035	1.07	0.935	0.0229	0.321	1.76
FLG	F	350	3.90	2.72	0.029	0.74	0.557	0.0267	0.271	6.96
FLG	F	450	0.31	0.352	0.018	0.14	0.077	0.0377	0.033	10.49
FLG	F	550	0.00	0.100	0.000	0.01	0.009	0.0335	0.002	-

Table I-2. DBP concentration measured from each subsite. DBPs not shown in this table exhibited concentrations too low for interest. Values displayed for DBP concentrations are the average of n=4 experimental replicates.

Site	Subsite	Temp (°C)	CHCl3 (µg/L)	TCAA (µg/L)	DCAA (µg/L)	TCP (µg/L)	DCAN (µg/L)	Chloropicrin (µg/L)
NED	A	0	64.09	72.08	36.93	1.86	0.95	1.45
NED	A	150	129.95	176.41	89.26	6.11	2.70	1.90
NED	A	250	561.10	853.29	463.61	20.08	28.87	1.55
NED	A	350	155.97	360.53	290.81	1.93	11.42	1.59
NED	A	450	10.05	28.29	31.69	0.31	0.75	0.19
NED	A	550	0.00	0.00	0.00	0.00	0.00	0.00
NED	B	0	127.58	167.88	98.63	2.24	2.51	5.16
NED	B	150	267.45	313.71	155.94	10.64	14.16	7.03
NED	B	250	749.92	840.07	438.05	23.23	76.10	1.92
NED	B	350	126.09	304.51	428.94	1.03	20.49	2.73
NED	B	450	8.32	35.47	78.94	0.00	2.67	0.24
NED	B	550	0.00	0.00	0.00	0.00	0.00	0.00
NED	C	0	244.10	253.49	142.70	5.67	6.17	4.11
NED	C	150	378.10	376.82	178.59	13.45	19.75	4.72
NED	C	250	1080.94	1353.11	625.57	20.08	141.69	2.01
NED	C	350	144.20	384.24	547.97	1.16	41.61	3.09
NED	C	450	8.64	34.39	83.79	0.00	3.06	0.16
NED	C	550	0.00	0.00	0.00	0.00	0.00	0.00
FLG	D	0	154.48	156.69	76.51	3.98	2.73	2.13
FLG	D	150	303.48	377.73	184.45	15.50	9.22	2.34
FLG	D	250	426.79	633.44	348.47	13.15	14.55	1.09
FLG	D	350	85.69	210.63	233.23	0.87	15.67	1.10
FLG	D	450	1.82	15.93	39.46	0.00	0.73	0.00
FLG	D	550	0.00	0.00	0.00	0.00	0.00	0.00
FLG	E	0	163.58	178.33	96.73	3.61	2.30	2.03
FLG	E	150	392.04	483.65	206.68	15.20	10.68	2.74
FLG	E	250	817.30	1030.27	566.07	21.96	55.21	1.58
FLG	E	350	115.56	303.32	427.17	0.83	18.86	1.86
FLG	E	450	6.66	40.75	86.97	0.00	1.91	0.00
FLG	E	550	0.00	0.00	0.00	0.00	0.00	0.00
FLG	F	0	273.98	321.99	150.81	5.05	4.71	2.39
FLG	F	150	799.00	790.35	400.68	31.96	16.05	3.17
FLG	F	250	329.01	500.06	365.58	6.95	15.38	1.06
FLG	F	350	61.20	229.97	425.73	0.00	13.87	1.90
FLG	F	450	4.43	23.60	69.51	0.00	0.94	0.00
FLG	F	550	0.00	0.00	0.00	0.00	0.00	0.00

Table I-3. DBP yields displayed also displayed in Figures 2-3 and 2-4. Subsite DBP yields were calculated by dividing the DBP concentration by the DOC concentration for every n=4 experimental replicate, and subsequently averaging these four values. NED DBP yield was calculated by averaging the DBP yield from Subsites A, B, and C. FLG DBP yield was calculated the same way, except with sites D, E, and F. It is important to note that dividing DOC or DON values from Table I-1 by DBP concentrations from Table I-2 will yield slightly different values

Site	Temp (°C)	CHCl3 (µg DBP/mg DOC)	TCAA (µg DBP/mg DOC)	DCAA (µg DBP/mg DOC)	TCP (µg DBP/mg DOC)	DCAN (µg DBP/mg DOC)	Chloropicrin (µg DBP/mg DOC)	SUVA 254 (L/mg m)
NED	0	43.2	50.1	27.7	1.02	13.4	18.4	2.07
NED	150	27.7	32.5	16.1	1.13	20.1	8.53	1.41
NED	250	44.5	57.8	29.6	1.47	37.7	1.00	3.88
NED	350	24.4	59.4	69.1	0.243	26.7	2.90	6.50
NED	450	18.2	66.6	131	0.208	12.2	1.72	6.50
NED	550	0.00	0.00	0.00	0	0.00	0.00	-
FLG	0	59.6	65.6	32.5	1.29	16.3	11.3	2.67
FLG	150	57.3	63.1	30.3	2.40	21.4	5.04	2.47
FLG	250	47.8	66.2	38.0	1.32	24.0	1.17	3.46
FLG	350	26.5	73.7	104	0.186	27.9	2.61	6.98
FLG	450	12.5	79.9	200	0	9.05	0.00	9.72
FLG	550	0.00	0.00	0.00	0	0.00	0.00	-

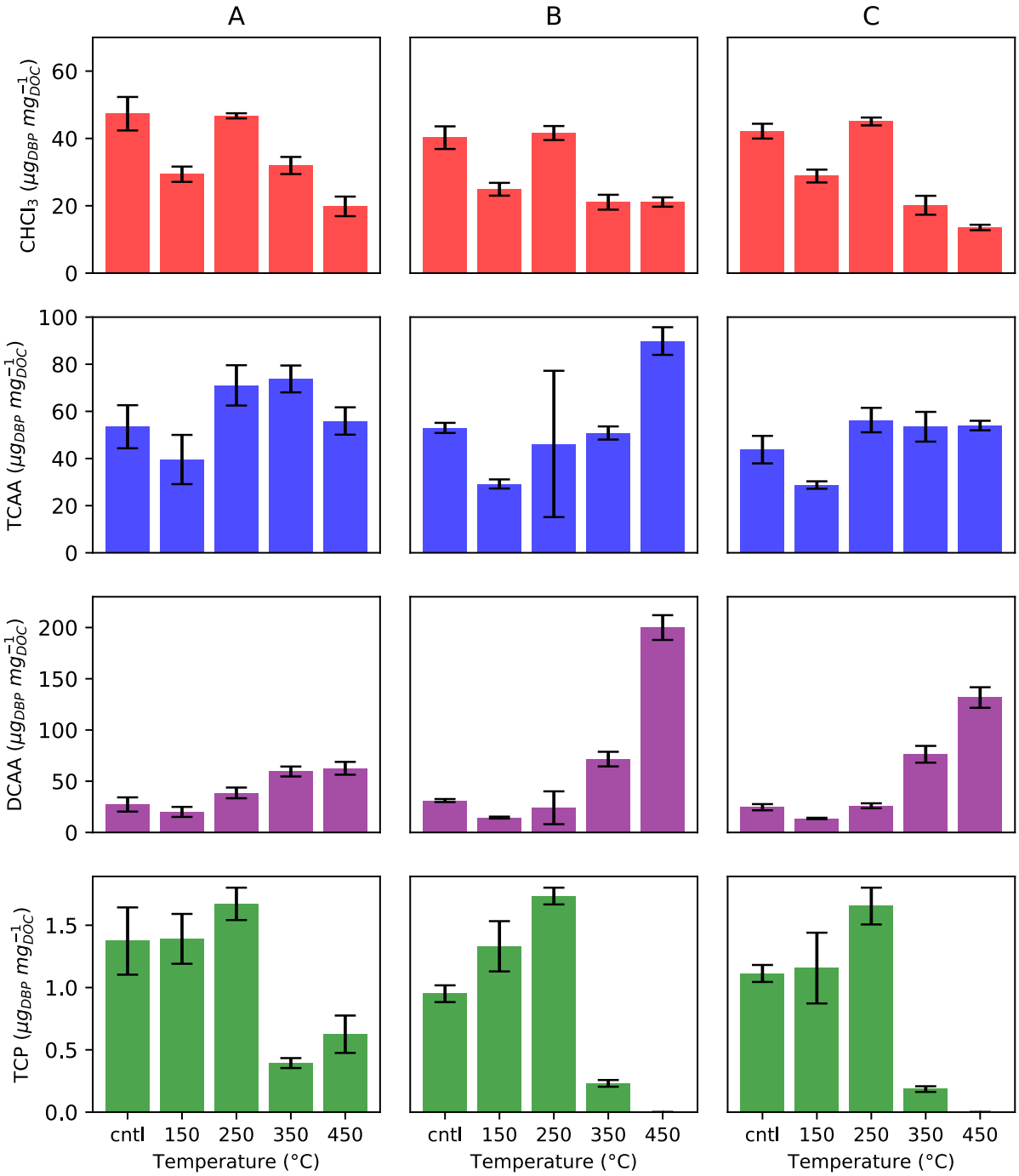

Figure I-1. C-DBP yield for the three subsites (A, B, and C) at NED. Error bars represent the propagated error calculated from four experimental replicates.

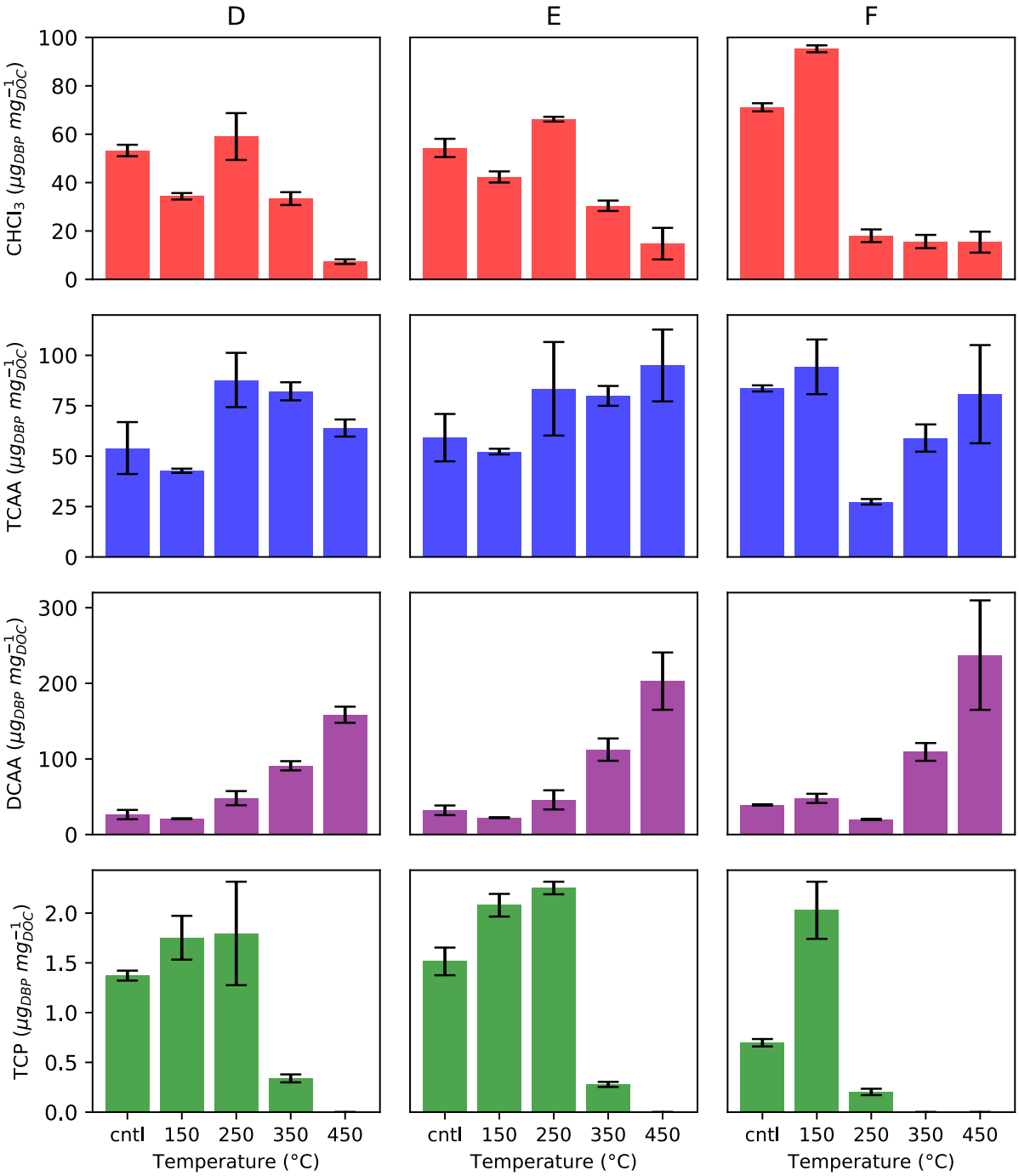

Figure I-2. C-DBP yield for the three subsites (D, E, and F) at FLG. Error bars represent the propagated error calculated from four experimental replicates.

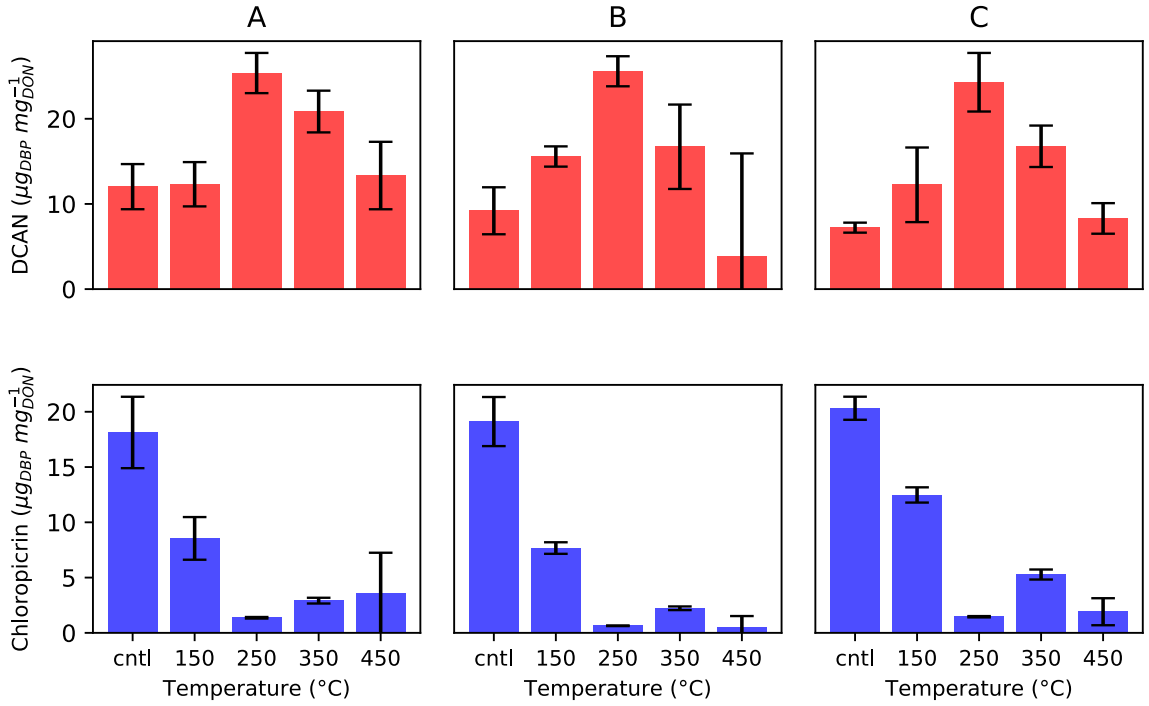

Figure I-3. N-DBP yield for the three subsites (A, B, and C) at NED. Error bars represent the propagated error calculated from four experimental replicates.

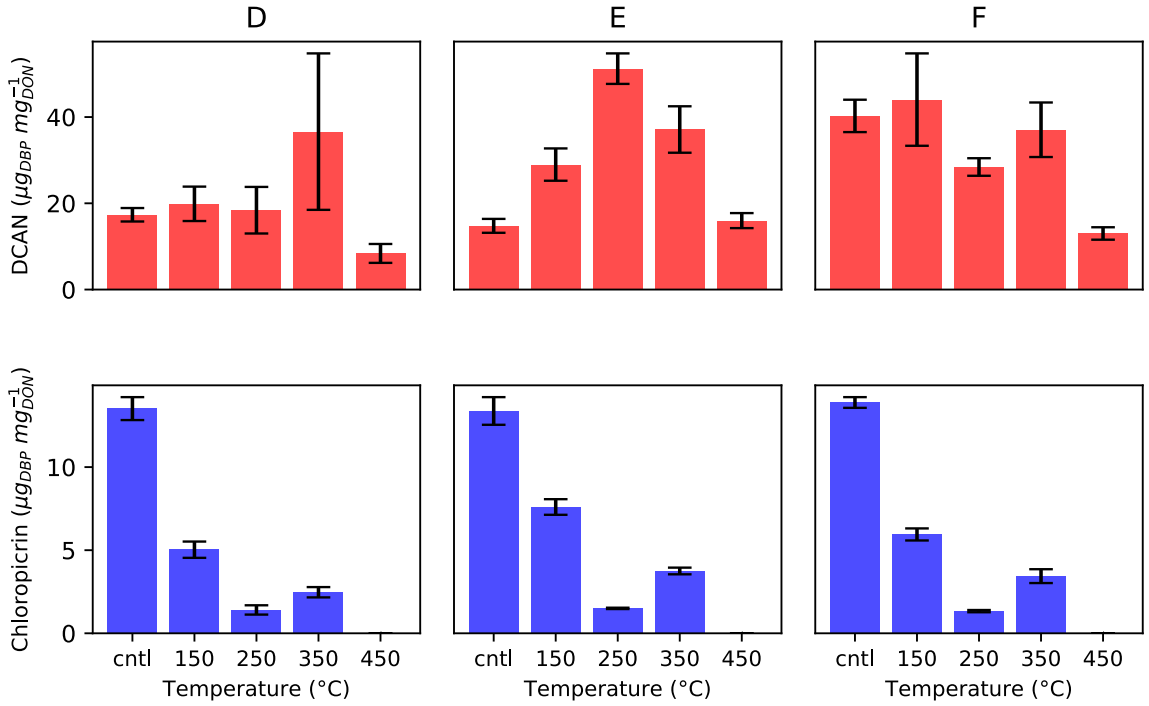

Figure I-4. N-DBP yield for the three subsites (D, E, and F) at FLG. Error bars represent the propagated error calculated from four experimental replicates.

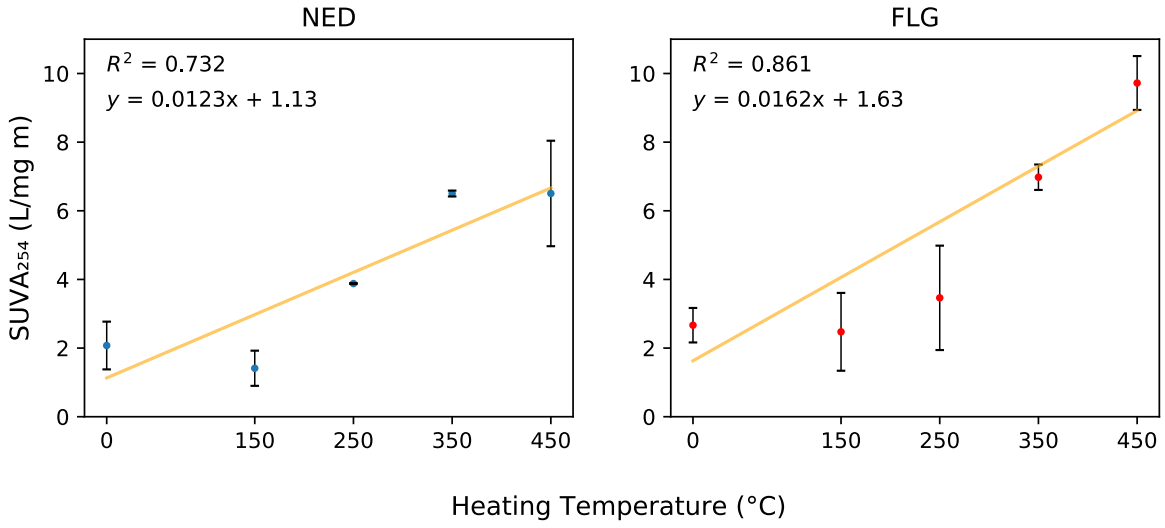

Figure I-5. Linear regression developed between $SUVA_{254}$ and heating temperature. Unlike figure 2-5, this figure includes $SUVA_{254}$ data for unburned control samples. Note that the linear relationships shown in this figure are poorer than the ones shown in figure 2-5. P-values for the intercept and coefficient can be viewed in table I-4.

Table I-4. Linear regression p-values associated with figure 2-4 and I-5. "No control" indicates that control $SUVA_{254}$ data was removed from the linear regression.

Site	p_{int}	p_{coef}
NED	0.076	4.67E-05
NED (no control)	-	3.90E-09
FLG	0.152	3.84E-05
FLG (no control)	-	3.00E-09

Table I-5. Linear regression p-values associated with Figure 2-5.

Site	p-value type	CHCl3	TCAA	DCAA
NED	p_{int}	2.42E-06	2.20E-04	-
NED	p_{coef}	3.77E-02	5.36E-02	3.19E-08
FLG	p_{int}	6.88E-05	6.95E-05	4.87E-03
FLG	p_{coef}	3.04E-02	4.42E-02	3.20E-09

Table I-6. Optical property data adapted from McKay et al. (2020).

Site	NED	SUVA (L/mg m)	SpA (RU L/mg_{DOC})	SpC (RU L/mgDOC)	Apparent Fluor. Quantum Yield (nm)
NED	0	3.1	0.5	0.2	0.0147
NED	150	1.7	0.2	0.1	0.0133
NED	250	4.3	1.4	0.7	0.0286
NED	350	4.5	3.6	1.6	0.0827
NED	450	9.4	12.7	5	0.108
FLG	0	2.5	0.4	0.1	0.0131
FLG	150	1.9	0.2	0.1	0.0111
FLG	250	4.2	1.8	0.9	0.0406
FLG	350	7.4	6.8	2.9	0.0992
FLG	450	12.6	8.4	3.9	0.0652

Table I-7. Two sample, two-tailed t-test p-values used for determining significant differences between DOC and DON concentrations at various temperatures.

Subsite	Comparison	DOC	DON
A	cntl/150	1.13E-05	4.68E-03
A	150/250	3.24E-06	1.61E-07
A	250/350	1.70E-05	2.05E-06
A	350/450	9.02E-05	4.23E-05
A	450/550	5.03E-06	4.84E-03
A	cntl/250	1.48E-09	7.02E-06
A	cntl/350	6.20E-05	5.45E-05
A	cntl/450	1.71E-04	7.59E-02
A	cntl/550	7.98E-05	1.04E-03
B	cntl/150	7.09E-09	3.83E-07
B	150/250	1.18E-04	1.62E-05
B	250/350	2.18E-05	5.96E-05
B	350/450	2.39E-06	8.20E-04
B	450/550	8.13E-08	3.46E-01
B	cntl/250	1.83E-05	1.30E-05
B	cntl/350	1.18E-06	1.07E-09
B	cntl/450	6.65E-07	1.67E-01
B	cntl/550	8.77E-07	3.00E-05
C	cntl/150	5.70E-05	2.75E-05
C	150/250	3.38E-07	1.84E-06
C	250/350	6.90E-07	1.82E-05
C	350/450	8.93E-06	4.19E-08
C	450/550	1.14E-05	2.64E-03
C	cntl/250	5.16E-07	6.54E-06
C	cntl/350	1.17E-04	4.75E-09
C	cntl/450	1.81E-05	1.27E-03
C	cntl/550	1.50E-05	8.21E-07

Table 1-7 cont.

Subsite	Comparison	DOC	DON
D	cntl/150	1.06E-06	7.72E-04
D	150/250	2.97E-02	1.83E-02
D	250/350	1.42E-03	1.51E-02
D	350/450	1.71E-05	3.99E-05
D	450/550	2.85E-06	5.69E-03
D	cntl/250	1.93E-03	3.35E-03
D	cntl/350	3.38E-03	7.65E-04
D	cntl/450	1.48E-07	1.11E-02
D	cntl/550	1.18E-08	6.97E-05
E	cntl/150	5.56E-05	6.47E-05
E	150/250	4.66E-05	1.55E-08
E	250/350	5.71E-07	6.76E-05
E	350/450	4.45E-06	6.16E-08
E	450/550	1.79E-03	2.67E-07
E	cntl/250	4.87E-10	5.23E-07
E	cntl/350	1.13E-03	3.87E-09
E	cntl/450	2.82E-08	2.57E-03
E	cntl/550	1.01E-05	6.97E-05
F	cntl/150	1.06E-10	1.56E-04
F	150/250	4.30E-08	7.34E-05
F	250/350	3.09E-08	1.07E-04
F	350/450	8.22E-05	2.73E-05
F	450/550	7.00E-03	2.18E-05
F	cntl/250	1.62E-08	6.90E-05
F	cntl/350	7.92E-01	1.30E-04
F	cntl/450	7.52E-09	4.51E-04
F	cntl/550	1.31E-06	9.59E-08

Table I-8. Two sample, two-tailed t-test p-values used for determining significant differences between NED DBP yields at different heating temperatures.

	NED					
	CHCl3 yield	**TCAA yield**	**DCAA yield**	**1,1,1-TCP yield**	**DCAN yield**	**Chloropicrin yield**
cntl/150	4.61E-09	5.65E-06	3.03E-06	4.24E-01	1.35E-02	7.85E-04
cntl/250	5.59E-01	2.77E-01	6.73E-01	1.11E-03	1.80E-05	1.14E-05
cntl/350	2.60E-08	4.39E-02	8.25E-11	4.73E-06	1.12E-04	2.96E-05
cntl/450	7.73E-13	1.37E-02	8.35E-05	4.51E-06	7.95E-01	7.50E-06
cntl/550	6.45E-12	7.40E-10	3.68E-09	8.83E-07	5.94E-08	7.14E-06
150/250	2.95E-14	1.02E-03	1.41E-03	1.74E-03	4.73E-04	2.30E-08
250/350	3.45E-08	8.21E-01	3.68E-09	1.19E-13	1.78E-02	4.91E-14
350/450	7.59E-03	2.49E-01	3.95E-03	7.33E-01	7.80E-03	1.94E-01
450/550	4.46E-09	5.45E-08	9.83E-06	4.65E-02	1.45E-02	6.68E-02

Table I-9. Two sample, two-tailed t-test p-values used for determining significant differences between FLGDBP yields at different heating temperatures.

	FLG					
	CHCl3 yield	**TCAA yield**	**DCAA yield**	**1,1,1-TCP yield**	**DCAN yeild**	**Chloropicrin yield**
cntl/150	7.97E-01	7.72E-01	6.20E-01	4.67E-03	3.78E-03	8.34E-08
cntl/250	1.08E-01	9.54E-01	2.70E-01	9.03E-01	4.02E-02	2.66E-09
cntl/350	2.44E-09	1.65E-01	3.07E-13	1.43E-14	1.25E-02	1.18E-08
cntl/450	4.94E-12	6.25E-02	1.62E-07	3.14E-14	2.60E-04	1.19E-09
cntl/550	7.97E-11	2.12E-08	5.26E-09	3.14E-14	1.71E-07	1.19E-09
150/250	3.67E-01	7.90E-01	2.00E-01	9.31E-03	4.81E-01	2.39E-11
250/350	7.69E-03	4.45E-01	7.01E-11	1.54E-04	4.52E-01	3.05E-14
350/450	7.63E-05	3.48E-01	3.68E-05	1.19E-03	5.33E-04	1.17E-13
450/550	2.58E-06	1.92E-08	3.30E-08	0.00E+00	4.60E-07	0.00E+00

Table I-10. Two sample, two-tailed t-test p-values used for determining significant differences between FLG DBP yield and NED DBP yield.

Comparison	**CHCl3**	**TCAA**	**DCAA**	**TCP**	**DCAN**	**Chloropicrin**
NED cntl/FLG cntl	0.092	0.225	0.328	0.291	0.512	0.225
NED 150/FLG 150	0.261	0.188	0.240	0.210	0.578	0.191
NED 250/FLG 250	0.846	0.718	0.460	0.777	0.302	0.866
NED 350/FLG 350	0.771	0.238	0.016	0.675	0.457	0.254
NED 450/FLG 450	0.180	0.419	0.227	0.422	0.660	0.057

Appendix II – Chapter 3 Data

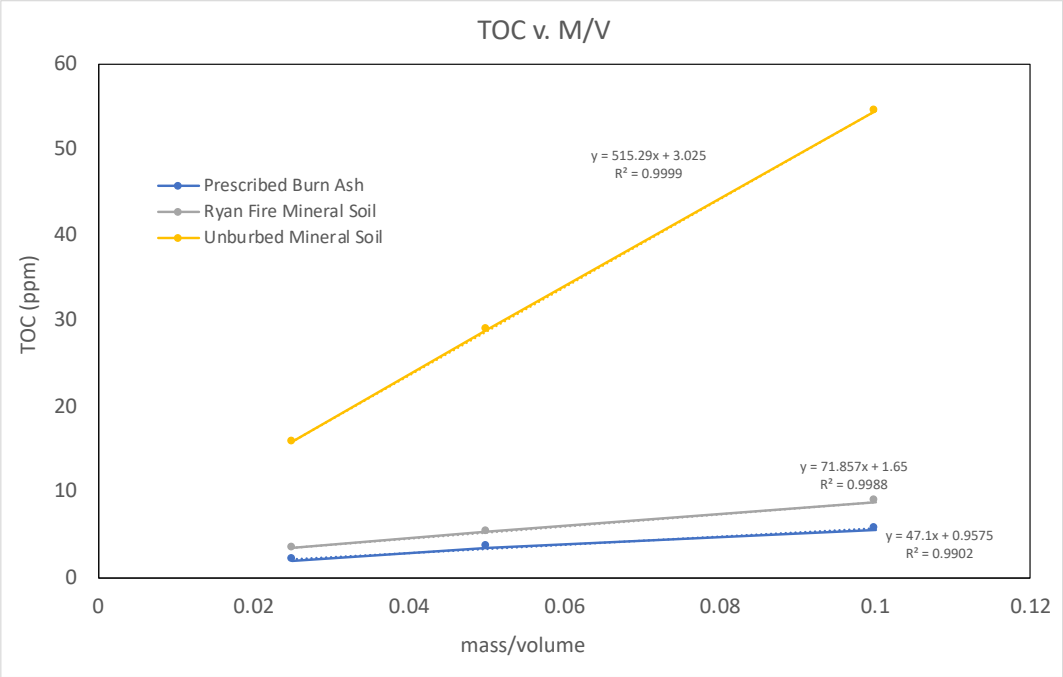

Figure II-1. Linearity test used to determine a mass/volume ratio for leaching Ryan Fire mineral soil and ash samples. Mass units are in g, while volume is in mL.

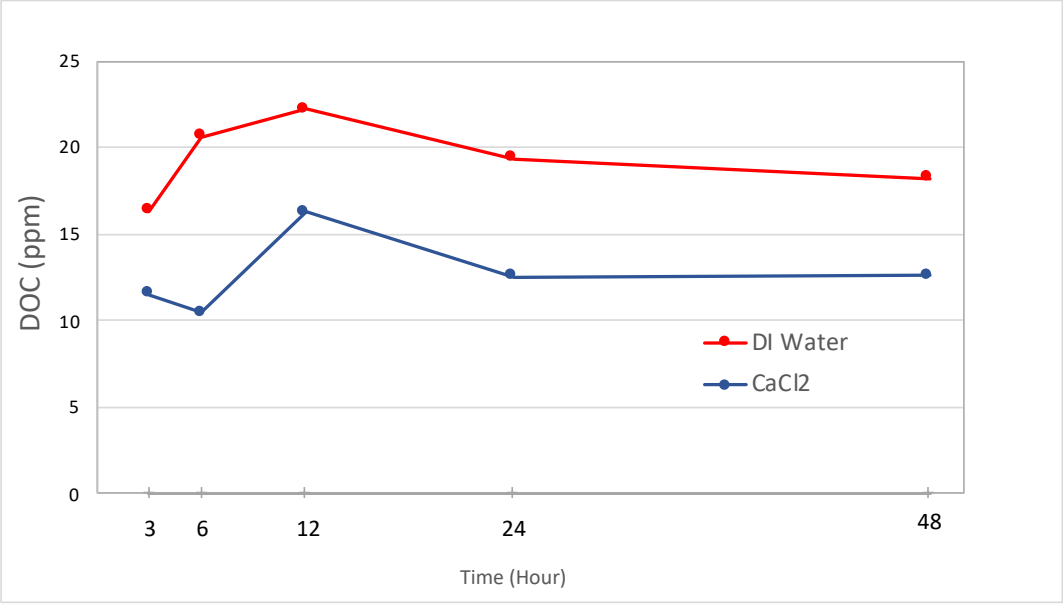

Figure II-2. Kinetics test used to determine the optimal leaching time. Twelve hours was chosen due to the maximum DOC concentration occurring at this time interval. The decrease measured between twelve and 48 hours could be due to instrument accuracy or sorption of DOC to the walls of the plastic centrifuge tube.

Table II-1. Summary table of pH, DOC, and heavy metals concertation normalized to soil mass. It is important to note that the mass/volume was ratio was constant for all samples. Error is the standard deviation calculated from three experimental replicates.

			Metal (μg/g)								
Sample	**pH**	**DOC (mg/g)**	**Al**	**Cd**	**Co**	**Cu**	**Fe**	**Mn**	**Ni**	**Pb**	**Zn**
OG Ash	6.55 ± 1.41	7.31 ± 0.908	199 ± 341*	< MDL	1.82 ± 2.75	1.65 ± 1.11	65.3 ± 117	2320 ± 463*	2.63 ± 4.18	< MDL	132 ± 33.0*
YF Ash	7.82 ± 0.108	2.05 ± 0.175	3.58 ± 0.302	< MDL	< MDL	< MDL	< MDL	400 ± 81.5*	< MDL	< MDL	66.8 ± 12.0*
Unburned Org.	7.16 ± 0.248	10.1 ± 1.55	20.5 ± 13.0	< MDL	< MDL	0.870 ± 0.358	7.75 ± 5.70	365 ± 413*	< MDL	< MDL	192 ± 50.3*
OG Min	5.57 ± 0.598	3.68 ± 0.824	324 ± 207*	< MDL	5.00 ± 2.88	1.06 ± 0.788	365 ± 263	768 ± 560*	4.50 ± 1.23	< MDL	142 ± 17.2*
YF Min	5.15 ± 1.09	2.73 ± 2.73	92.6 ± 135*	< MDL	0.574 ± 0.690	0.663 ± 0.445	69.8 ± 114	199 ± 139*	2.16 ± 0.870	< MDL	193 ± 124*
Unburned Min.	5.05 ± 1.23	3.51 ± 0.607	429 ± 379*	1.53 ± 1.14	1.33 ± 0.583	3.68 ± 3.23	38.5 ± 9.95	713 ± 688*	8.45 ± 4.45	0.513 ± 0.340	223 ± 106*

*Samples with at least one experimental replicate that exceeded the instrument calibration curve range

Table II-2. P-values associated with the two sample, two tailed t-tests performed between the various sample types.

Sample	pH	DOC	Al	Cd	Co	Cu	Fe	Mn	Ni	Pb	Zn
OGAsh/OGMin	0.334	**0.007**	0.618	0.263	0.238	0.492	0.147	**0.021**	0.497	0.320	0.676
OGAsh/UnbOrg	0.500	**0.05**	0.415	0.614	0.324	0.363	0.441	**0.005**	0.432	0.395	0.159
OGMin/UnbMin	0.547	0.79	0.694	0.184	0.095	0.244	0.099	0.82	0.213	0.241	0.26
YFAsh/YFMin	**0.014**	0.687	0.316	0.174	0.199	0.474	0.337	0.095	**0.017**	0.093	0.155
YFAsh/UnbOrg	**0.014**	**<0.001**	0.088	**<0.001**	**0.023**	0.097	**0.043**	0.892	**<0.001**	**0.001**	**0.014**
YFMin/UnbMin	0.922	0.653	0.221	0.144	0.31	0.185	0.661	0.333	0.075	0.073	0.763
OGAsh/YFAsh	0.196	**0.006**	0.376	0.293	0.343	0.137	0.374	**0.002**	0.37	0.316	0.320
OGMin/YFMin	0.591	0.593	0.181	0.507	0.066	0.492	0.151	0.162	0.055	0.069	0.521
UnbOrg/UnbMin	**0.044**	**0.002**	0.135	0.130	0.184	0.221	**0.010**	0.581	0.368	0.068	0.671